

REMANENT CREEP LIFE PREDICTION
IN LOW-ALLOY FERRITIC STEEL
POWER PLANT COMPONENTS

By
Peter Wilson
Pembroke College
Cambridge

A dissertation submitted for the degree of
Doctor of Philosophy
at the University of Cambridge
November 1990

PREFACE

This dissertation is submitted for the Degree of Doctor of Philosophy in the University of Cambridge. The investigation described herein was carried out under the supervision of Dr H.K.D.H. Bhadeshia in the Department of Materials Science and Metallurgy, University of Cambridge, between October 1986 and September 1990.

Except where acknowledgement and reference is specifically made to the contrary, this work is, to the best of my knowledge, original and has been carried out without collaboration. Neither this, nor any substantially similar dissertation has been, or is being, submitted for any degree, diploma or other qualification at any other university.

This dissertation does not exceed 60 000 words in length.

A handwritten signature in black ink, appearing to read 'Peter Wilson', with a long horizontal flourish extending to the right.

Peter Wilson

Pembroke College

November 1990

ACKNOWLEDGEMENTS

I am indebted to Dr H.K.D.H. Bhadeshia for his invaluable advice and support during the course of this research, and to Professor D. Hull for the provision of laboratory facilities in the Department of Materials Science and Metallurgy at the University of Cambridge.

I must also express my gratitude to friends and colleagues in the Department, and especially in the Phase Transformations Group, in particular to Dr Jer-Ren Yang and Dr Serdar Atamert for their advice on practical techniques during the earlier stages of my research.

Thanks are also extended to the technical staff of the department, particularly Mr John Leader for technical guidance with dilatometry, Mr Dave Nichol for his help and advice on electron microscopy and carbon replica preparation, Mr Brian Barber for his photographic services, and Messrs David Duke, Graham Morgan, Paul Stokes and the workshop staff who provided much valuable technical assistance.

This work was supported by the Central Electricity Generating Board, and my thanks are extended to them. Particular gratitude is expressed to Dr David Gooch of the National Power Technology and Environment Centre (NPTEC) for the interest he has shown in the project, and to Martin Askins and Jackie Maguire for guidance and help during visits to NPTEC.

CONTENTS

Preface	i
Acknowledgements	ii
Table of Contents	iii
Abstract	v
Abbreviations	vii
List of symbols	ix
Chapter 1: Introduction to Remanent Life Prediction	1
1.1 Problems With High-Temperature Plant Operation	1
1.2 The Need for Accurate Life Prediction	2
1.3 Plant Life Extension: British Experience	3
1.4 Plant Life Extension: Critical Areas	4
1.5 Materials and Conditions	9
1.6 Current Remanent Life Assessment Procedures	12
1.7 Methods Based on Operational Data Monitoring	15
1.8 Methods Using Post-Service Material	24
Chapter 2: Microstructure of Creep Resistant Low-alloy Ferritic Steels	34
2.1 The Austenite–Ferrite Transformation	34
2.2 The Bainite Transformation	41
2.3 Carbide Precipitation in Allotriomorphic Ferrite	50
2.4 Changes in Alloy Carbides Within Ferrite During Ageing	55
2.5 Cavitation During Creep	59
2.6 Ageing Behaviour of Bainitic Cementite	61
Chapter 3: Characterization of Pre-Service Microstructure	70
3.1 Introduction	70
3.2 Optical Metallography	70
3.3 Quantitative Metallography	75
3.4 Hardness Measurements	77
3.5 Energy Dispersive X-ray Analysis	81
3.6 Summary	85
Chapter 4: Modelling the Austenite–Ferrite Transformation	87
4.1 Introduction	87
4.2 Theoretical Calculation of TTT Diagrams	88
4.3 Calculation of Phase Diagrams	93
4.4 Heat Treatments on Steam Header Section	94
4.5 Results of Dilatometric Experiments	98
4.6 Metallographic Examination of Heat Treated Specimens	117
4.7 Summary	119

Chapter 5: Ageing of Bainitic Microstructures:	
Experimental procedure	126
5.1 Introduction	126
5.2 Programme of Heat Treatments	126
5.3 Procedure for Microanalysis	129
5.4 Interpretation of Microanalytical Data	134
Chapter 6: Ageing of Bainitic Microstructures:	
Fe-Cr-Mo Steel	144
6.1 EDX Compositional Data	144
6.2 Variation of Composition Change with Particle Size	146
6.3 Variation of c^θ with Time: Analytical Approach	184
6.4 Theoretical Modelling of the Ageing Process	195
6.5 A Finite Element Analysis of the Ageing Process	202
6.6 Variation of c^θ with Time: Finite Difference Approach	209
6.7 Alloy Carbide Precipitates	217
6.8 Summary	218
Chapter 7: Ageing of Bainitic Microstructures:	
Fe-Cr Model Alloy	220
7.1 EDX Compositional Data	221
7.2 Variation of Composition Change with Particle Size	222
7.3 Variation of c^θ with Time	228
7.4 Alloy Carbide Precipitates	234
7.5 Summary	236
Chapter 8: Summary	241
8.1 Composition Changes During Ageing of Bainitic Cementite	241
8.2 Remanent Life Prediction	243
References	245
Appendix 1: Steels Used in the Programme	251
Appendix 2: Program to Simulate Stochastic Scatter in EDX Composition Analysis	254
Appendix 3: Finite Difference Program to Analyse Ageing of Bainitic Cementite	257

ABSTRACT

It is believed that the safe creep life of low-alloy steel components used in the boiler systems of power stations has in the past been underestimated. The underestimation arises in part from inaccuracies associated with current predictive techniques, and in part due to variations in service conditions which are difficult to monitor (and may, at times, exceed the design specifications). A large incentive for producing more accurate creep life estimates is provided by the imminent closure of large quantities of power plant (due to life exhaustion on the basis of current estimates). The work in the current project had its origin in this engineering problem, and in particular in addressing the problem of accurate determination of the temperature regime experienced by these materials in service, when operating temperatures are known to be subject to fluctuation.

It has been suggested by a number of authorities that measurements of compositional changes which occur in carbides within the material during ageing could, if coupled with a rigorous theory predicting enrichment rates, produce a more representative indication of the true thermal history of the component than has been possible to date. This would provide a particularly powerful technique in relation to extending the service life of existing plant, as it is essentially non-destructive. The major aim of the current work has been to characterize those precipitates which are found in these alloy systems and, by carrying out EDX compositional analysis of aged specimens, to test and develop a model for the enrichment process which is more fundamentally-based and representative than the largely-empirical models commonly used in industrial practice.

In chapter one of this dissertation an analysis is made of the problem of remanent life prediction in engineering terms, with particular emphasis on the sources of approximation in current estimates. Chapter two considers the available theory to explain the development of creep-resistant microstructures in low-alloy steels during component fabrication, and the subsequent microstructural changes which occur in these steels during ageing under service conditions. Particular emphasis is given to the question of cementite enrichment with sub-

stitutional alloying elements, and it is noted that recent work based on diffusion theory predicts enrichment which varies as $(\text{time})^{1/2}$, a result which contrasts with relations of a $(\text{time})^{1/3}$ form which have hitherto been applied industrially.

In chapter three, the microstructure of a typical example of a $1\text{Cr}\frac{1}{2}\text{Mo}$ power plant steel in the as-fabricated condition is examined and discussed. Chapter four involves the study of the austenite–ferrite transformation in this steel, both on the basis of current phase transformation theory and by dilatometric experiment.

The procedure used for determining composition changes which occur during ageing is outlined in chapter five, and the results discussed and analysed in chapters six and seven. Chapter six compares enrichment of cementite by substitutionals in the $1\text{Cr}\frac{1}{2}\text{Mo}$ steel with theoretical predictions based on both an analytical model which considers the rate of enrichment to be controlled by diffusion within a semi-infinite ferrite matrix to the α/θ interface, and a finite difference method which takes account of the finite inter-cementite spacing, and hence of soft impingement effects. A good correlation is found between experiment and theory: in particular, enrichment occurs in accordance to a $(\text{time})^{1/2}$ relationship, and the level of enrichment at a given time is found to vary as the reciprocal of the particle size. Chapter seven analyses enrichment in a higher-chromium alloy in which precipitation of another alloy carbide species (M_7C_3) at the expense of cementite takes place during ageing; thus, the effect of this on cementite enrichment can be examined.

In chapter eight, some general conclusions are drawn, a consideration given to the possible applicability of measurements of this type to the remanent life question, and suggestions for future work are made.

ABBREVIATIONS

bcc	body-centred cubic
BF	bright field
CAF	cavity area fraction
CCT	continuous cooling transformation
CEGB	Central Electricity Generating Board (of England & Wales)
CERL	Central Electricity Research Laboratories (of the CEGB)
CVN	Charpy V-notch
DF	dark field
EDX	energy dispersive X-ray analysis
fcc	face-centred cubic
GB	grain boundary
HAZ	heat affected zone
hcp	hexagonal close-packed
IPS	invariant plane strain
K-S	Kurdjumov-Sachs relationship
MDHS	mean diameter hoop stress
MTDATA	Metallurgical and Thermodynamic Data Service
NAG	Numerical Algorithms Group
NDT	non-destructive testing
NPLE	negligible-partitioning local equilibrium
OA	optic axis
ParaE	paraequilibrium
PS	proof stress
RCL	remanent creep life
RF	radio frequency
SADP	selected area diffraction pattern
SEI	secondary electron image/imaging
SEM	scanning electron microscopy
TEM	transmission electron microscopy
TTT	time-temperature-transformation

VHN	Vickers hardness number
YS	yield strength

LIST OF SYMBOLS

a	lattice parameter of cubic crystal
Ae_3	the temperature of the equilibrium $\alpha + \gamma/\gamma$ phase boundary
Ae'_3	the temperature of the para-equilibrium $\alpha + \gamma/\gamma$ phase boundary
B_s	bainite start temperature
C	non-dimension variable in finite element analysis associated with concentration
$C_{i,j}$	normalized composition of finite element i, j
c_x	concentration of element X
c^z	concentration in phase Z
\bar{c}	mean alloy composition
$c^{\alpha\theta}$	composition of ferrite in equilibrium with cementite
$c^{\theta\alpha}$	composition of cementite in equilibrium with ferrite
d	diameter
d_b	bore (inner) diameter of pipe
d_o	outer diameter
e	engineering strain or conventional strain
e_α	coefficient of linear thermal expansion of ferrite
e_γ	coefficient of linear thermal expansion of austenite
I	intensity
I'	observed intensity of EDX signal when reduced by absorption
k	partition coefficient
L	liquid
\bar{L}	mean linear intercept
l	length
l_0	initial length
M_s	martensite start temperature
P	steam pressure
T	temperature
t	time, pipe wall thickness

T'	non-dimension variable in finite element analysis associated with time
T_{amb}	ambient temperature
T_{aus}	austenitising temperature
t_{aus}	austenitising time
t_c	ageing time required to reach a given composition
t_f	time to failure
T_{hom}	homogenising temperature
T_{iso}	isothermal transformation temperature
T_s	service temperature
t_s	time at service conditions
$t_{s,f}$	time to failure at service conditions
T_t	test temperature
t_t	time at test conditions
$t_{t,f}$	time to failure at test conditions
$t_{t,f_{\text{ex}}}$	rupture time for service exposed material under test conditions
$t_{t,f_{\text{unex}}}$	rupture time for unexposed material under test conditions
T_0	original temperature, temperature at which α and γ of the same composition have the same free energy
T'_0	T_0 temperature adjusted to allow for 400 Jmol^{-1} strain energy
V	volume
V_{α_b}	Volume fraction of bainite
$V_{\alpha'}$	Volume fraction of martensite
$V_{\gamma_{\text{ret}}}$	Volume fraction of retained austenite
V_{α}	Volume fraction of allotriomorphic ferrite
W_s	Widmanstätten ferrite start temperature
wt %	proportion of element as percentage by weight
X	non-dimension variable in finite element analysis associated with distance
x_{θ}	thickness of cementite plate
α	ferrite, allotriomorphic ferrite

α	tilt angle in EDX technique
α_a	acicular ferrite
α_b	bainite
α_{lb}	lower bainite
α_{ub}	upper bainite
α_w	Widmanstätten ferrite
α'	martensite
β	elevation of EDX detector
γ	austenite
γ_{ret}	retained austenite
δ	delta-ferrite
Δ	difference
Δl	length change
Δl_{rel}	relative length change ($\Delta l / l_0$)
ΔT	temperature difference, undercooling
Δ_m^v	maximum volume free energy change for nucleation
ε	strain
$\dot{\varepsilon}$	strain rate
$\dot{\varepsilon}_m$	minimum creep strain rate
θ	cementite
θ	angle between detector and tilt axes in EDX technique
σ	stress
σ_{mdhs}	mean diameter hoop stress
σ_{ref}	reference stress
σ_s	service stress
σ_t	test stress
σ_1	maximum principal stress
$\sigma_{\theta\alpha}$	surface energy of cementite particle in ferrite
τ	transformation incubation time
ψ	EDX take-off angle
ω	creep damage parameter

Chapter 1

INTRODUCTION TO REMANENT LIFE PREDICTION

1.1 Problems With High-Temperature Plant Operation

Creep life assessment is essential for the determination of a safe operating life for high-temperature power plant. Furthermore, the accuracy of such assessments has a strong bearing on the economical operation of power stations; accurate life prediction allows the maximum safe use to be achieved with each component, whereas the lack of an accurate predictive model necessitates the use of expensively-large safety factors.

High-temperature component design codes are customarily based principally on uniaxial creep rupture data. Additionally, depending on operating conditions, cyclic creep, creep fatigue, environmental attack etc. may also be of significance. The base material is usually assumed to be chemically homogeneous, which is a further potential source of inaccuracies, and design codes must always be conservatively determined for safety reasons (Cane & Williams, 1987).

Evidence obtained from examinations of components removed from service, however, has shown that the safe creep design life of creep resistant low-alloy steels may have been underestimated significantly leading to the expense of unnecessary replacements. This problem is thought to arise in part as a result of inaccuracies in present predictive techniques (Cane & Townsend, 1984; Cane & Williams, 1987); in particular, the complexity of the systems and the harshness of the operating environment make the modelling procedure more complex.

Cane (1986) has found that a particularly significant inaccuracy arises from the use of standard creep data derived from small test samples whose behaviour in a given environmental condition would be expected to differ from that of the bulk component. An example of this is provided by the relative effect of oxidation on creep data for different thickness test pieces, which shows a specimen thickness dependence; oxidation effects are negligible for thick specimens, but of

increasing importance as the surface:volume ratio increases. A general discussion of the problems associated with the use of standard data and extrapolation to on-plant conditions is given in section 1.7.2.

It is also known that service conditions can be highly variable and, at times, exceed those allowed for in the design specifications, especially in localized areas. Cane and Townsend (1984) found variations of 30–40°C in exceptional circumstances, equivalent to an order of magnitude change in the creep lifetime of the material and thus a serious limiting factor on any remanent life¹ assessment.

A further source of imprecision in component lifetime prediction can be attributed to welds and weldments, where the complex microstructure and chemical inhomogeneity can lead to a non-uniform stress distribution and sites of stress concentration where cavitation in the initial stage of creep can occur. Nevertheless, although such regions are critical for creep damage, they are not necessarily so in terms of life exhaustion; in many cases, non-destructive damage monitoring and repair are relatively easy for weldments. In consequence, most efforts directed at predicting remanent life are concentrated on the parent material. Accurate assessment of the problems in high-risk areas is of particular importance, so that critical components can be identified and carefully monitored (Price & Williams, 1982; Parker & Sidey, 1986); thus the locating of those areas where the creep environment is especially harsh must constitute a significant part of any remanent life prediction procedure.

1.2 The Need for Accurate Life Prediction

- (i) To satisfy the various safety standards demanded by legislating and licensing bodies, insurers *etc.*
- (ii) To avoid the large expense and risk of plant damage and serious injury to personnel associated with sudden high-temperature failures.

¹ Remanent creep life is the time remaining before creep induced failure occurs in a partially-creep-damaged artefact, such as a high-temperature component which has been exposed to service conditions for a fraction of the time in service which would result in creep rupture.

- (iii) To predict in advance when the need for component replacement is likely to arise in order to allow time for the manufacture of a replacement before it is needed in service. British experience suggests that for steam headers² advanced warning should ideally be three to four years, although for less specialised components this can be much reduced (Cane & Townsend, 1984).
- (iv) To allow safe extension of service life, and maximize plant usage.
- (v) To avoid complete replacement of existing plant and adopt instead where possible a repair/replace single components philosophy.

1.3 Plant Life Extension: British Experience

Realistic lifetime assessment is of particular interest to the large generating companies in the United Kingdom, because of their large capital investment in low-alloy ferritic steel plant. There have been very few catastrophic high-temperature failures recorded which have resulted in major steam leakage and serious plant damage or injury, but this is primarily due to the high degree of caution which must be employed in the field of creep life prediction specifically to avoid such failures. In many cases, this policy is found to lead to the premature decommissioning of plant and consequent loss of capital which makes representative remanent life prediction of substantive value in relation to extension of plant life (Gooch & Townsend, 1986).

The electricity generating industry in England and Wales has 54 000 MW of generating capacity, which includes twelve large stations comprised of 41 high-merit 500 MW coal fired units. These units are noted for their good thermal efficiency and low operating cost. Designed in the 1960s and 70s for 150 000 hour (25 year) operation, they have reached 90 000–120 000 hours of service each. A programme to increase plant life to 250 000 hours or more is thought to be feasible and two procedures to achieve this are proposed, by Townsend (1986), to form the basis of a plant life prolongation programme initiated by the Central Electricity Generating Board of England and Wales (CEGB):

² Steam headers are those parts of the boiler system of a power station which act as junctions between the simple boiler tubing. They can be very large and of complex design, hence the long replacement times noted above.

- (i) Replacement of all critical components at 150 000 hours;
- (ii) Predictive assessment coupled with a replacement of only those components shown to have a total potential lifetime of less than 250 000 hours.

In principle, the second solution is the more satisfactory as all components work through an entire useful life: in practical situations considerations including the engineering feasibility of life extension and the relative costs of the two options must also be factors in the question of replacement versus extension. It is likely that for cheap components which are easily replaced (*e.g.*, boiler tubes) the strategy outlined in option (i) will be favoured, whereas for more expensive and complex components (*e.g.*, steam headers) development of improved anticipatory techniques to allow life extension should be of economical benefit (Townsend, 1986).

In the case of the 12 large stations mentioned above, a strategy based on extending life could be practicable, as the original design remains relatively advanced in engineering terms with few technical improvements probable in the foreseeable future. This negates the principal value of new plant construction: improved efficiency achieved by incorporating improved design. A prolongation of working life to 40 years or more would produce considerable financial advantage: retaining current plant in service would be achieved at around one third of the cost of building new plant; and the many problems associated with siting new power stations (environmental concerns, lengthy public enquiries and so on) could also be avoided if the service life of existing power plant were lengthened significantly. Improvement of current predictive techniques is thus of great interest and potential value to the large scale electricity generation industry.

1.4 Plant Life Extension: Critical Areas

1.4.1 Power plant arrangement

The majority of the generating capacity in England and Wales produces electricity with a steam turbine arrangement, with various initial fuel sources (coal, oil, the nuclear pile *etc.*) being used to heat the steam. The basic furnace and

boiler arrangement of steam turbine generating plant is the same regardless of the fuel source used.

Water is supplied to the steam drum by feed pumps, usually passing through an economizer. This device is heated by hot gases from the furnace (as are the superheaters and reheaters (see below), thus enabling pre-heating of the feedwater). The water is drawn from the steam drum into tubes on the furnace walls, and returns to the drum as a mixture of water and steam. The water and steam are separated in the drum, and the water recycled to the furnace wall, with the steam passing on through the superheaters to the high-pressure cylinder where it is directed at the turbines, producing rotation. Exhaust steam from the high-pressure cylinder is passed through reheaters to get it back up to temperature, thence to the intermediate- and low-pressure cylinders to drive further turbines. A diagram of the general boiler and steam plant arrangement is given in figure 1.1.

1.4.2 Applicability of life extension to steam headers

Several components have been identified as being particularly susceptible to high-temperature failure, and these are listed in table 1.1 and figure 1.2. Accurate remanent creep life prediction would be conducive to improvement in overall operating lifetime assessment if concentrated in these areas.

On the basis of the criteria considered in Section 1.3, it is evident that boiler components, both for their complexity and cost, and for the harshness of the operating regime, are especially suited to a life extension programme. Moreover, the steam header is operated under a particularly severe service regime, especially in relation to localized heating to as much as 40–50°C over design temperature (which is 568°C); this arises mainly due to the complexity of the shape, which causes a highly irregular heat flow during operation. Localized heating above design specifications effects a more rapid exhaustion of creep life at those localized sites.

A recent CEGB survey indicated that nearly all steam header replacements are made as a result of exhaustion of design creep life. In only 25% of these

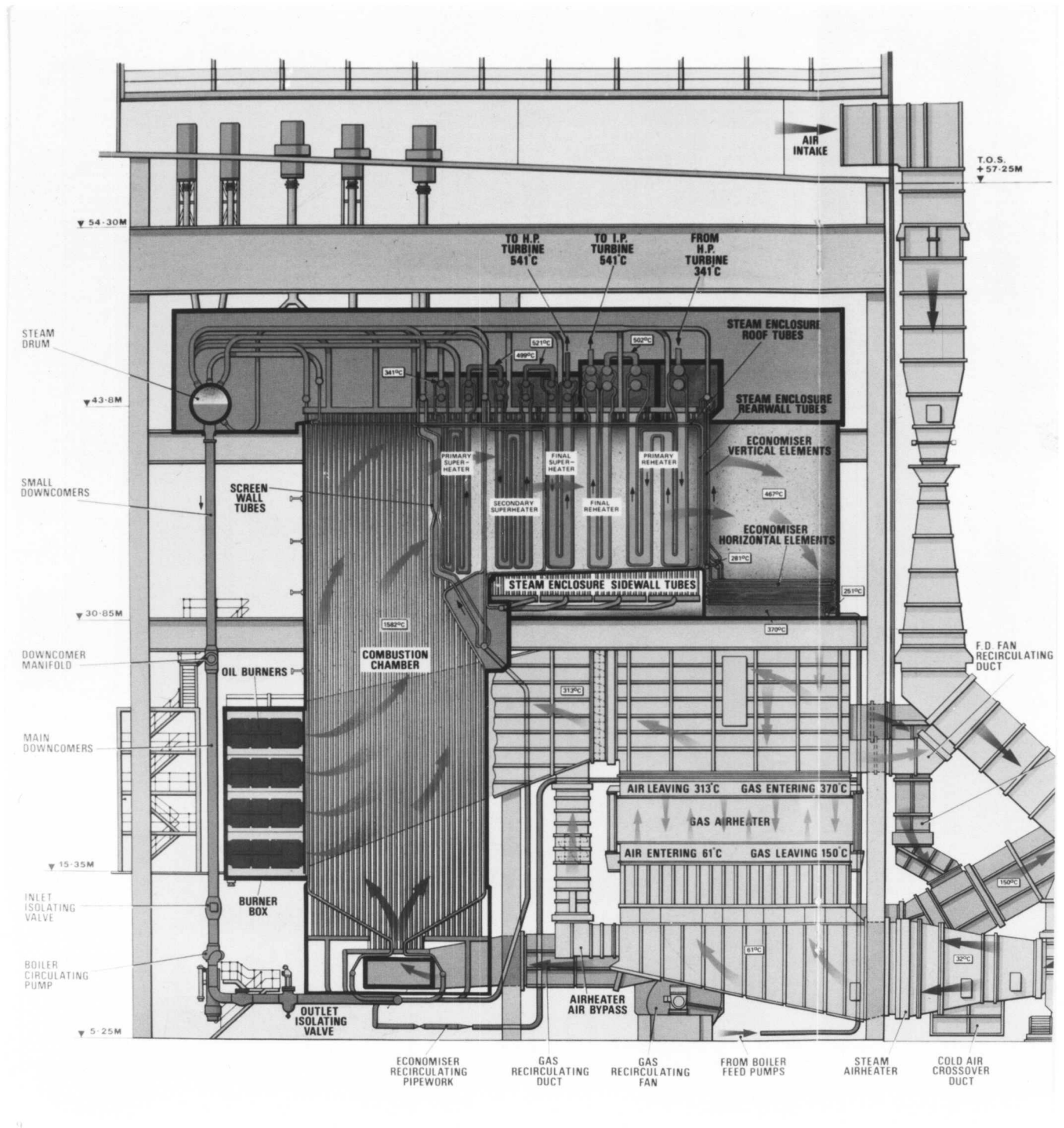


Figure 1.1: A power station boiler and associated steam plant (Littlebrook Power Station Guide, National Power Technical Publications)

Area		Materials	Life-limiting factor
<i>Boilers</i>	Drums	Carbon steels	Creep and thermal fatigue
	Headers	Carbon & Cr-Mo steels, austenitic stainless steels	Creep and thermal fatigue
	Furnace wall, superheater, reheater tubing	Carbon & Cr-Mo steels, austenitic stainless steels	Fireside and waterside corrosion
<i>Pipework</i>	Main and reheater pipes	Cr-Mo, Cr-Mo-V steels, austenitic stainless steels	Creep and thermal fatigue, weld and HAZ cracking
<i>Turbines</i>	All rotors	Cr-Mo-V (-Nb-W) steels	Creep and thermal fatigue
	Low pressure rotors and turbine blades	Ni-Cr-Mo-V steels	Fretting fatigue, corrosion fatigue, stress corrosion & pitting <i>etc.</i> , temper embrittlement
	Steam chests and casings	Cr-Mo, Cr-Mo-V steels	Creep & thermal fatigue
	Elevated temperature boltings	Cr-Mo-V (-B) steels, nickel based alloys	Creep and thermal fatigue stress corrosion

Table 1.1: Critical areas for high-temperature failure

cases was evidence of creep damage exhibited in the form of inlet stub tube weld cracking or swelling of the steam header body: many of the remainder were found to have significant potential service life left.

Cane and Townsend (1984) outline the specific problem that the Industry faces as a result of creep life exhaustion. Included in British generating plant are more than 300 headers which, on the basis of present creep life theories, will

typical areas of attention for plant life extension on coal

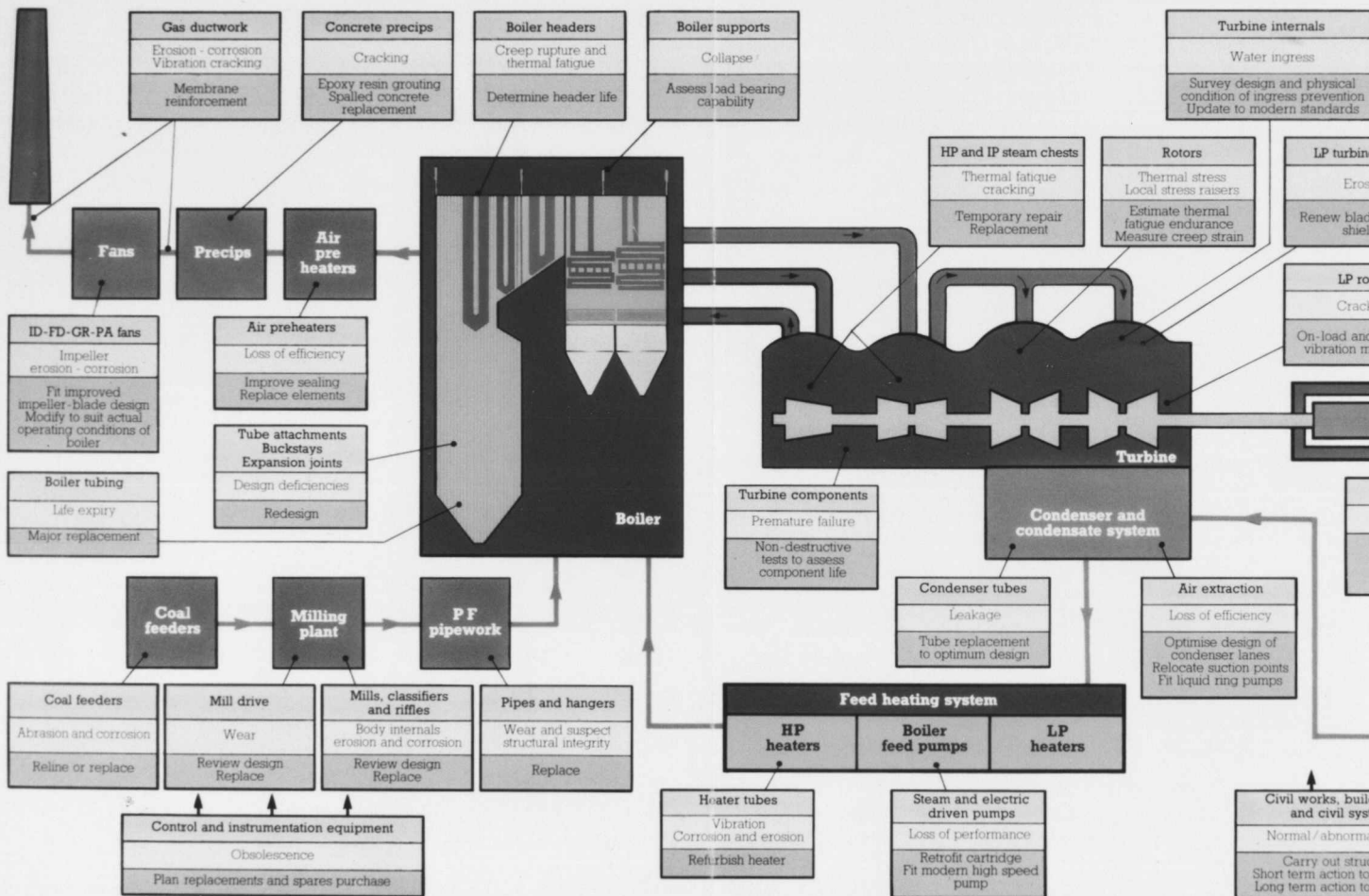


Fig 1.2

require replacement at some time during the next 25 years at a cost, in engineering terms alone, of some £170–£200 millions; thus, the financial incentive for extending safe creep life in this area is very large indeed. Furthermore, the absence of cost-effective and practicable alternative monitoring procedures that are applicable to steam headers, a problem not associated with most of the other critical areas listed in the table, provides further incentive for the development of predictive models; the header body is difficult to observe, expensive to replace, and, due to the complexities of its manufacture, must be ordered 2 years or more in advance of the need for replacement arising. Accurate anticipation of failure can avoid potentially disastrous long periods of plant repair, whilst at the same time reducing the financial and material wastage arising from unnecessary replacement. In contrast, other critical boiler components such as welded joints or boiler tubes are easier to inspect and repair; hence, in those cases, investment in remanent life research does not produce such high levels of return.

1.5 Materials and Conditions

1.5.1 *Materials used in current steam headers*

Of the more than 300 steam headers mentioned above as requiring replacement within 25 years, three are mild steel and the remainder are low-alloy ferritic steels. Chromium and molybdenum are the primary alloying elements in all of these steam headers, with vanadium also used in some more recent designs. The carbon content in all three of the alloys used is in the range 0.10–0.12 wt %. A breakdown of the currently-predicted replacement dates for the steels is given in figure 1.3. The figure applies to the larger headers (> 2 m length) which are a particular problem.

A breakdown of figure 1.3 reveals that ninety-five 1Cr– $\frac{1}{2}$ Mo class steel steam headers are due for replacement over the period, all within the next 15 years, and the bulk of the 126 $2\frac{1}{4}$ Cr–1Mo class steel headers of the $2\frac{1}{4}$ Cr–1Mo class steel which are due to be replaced by 2010 will also reach the end of their anticipated service life over the same 15 year period. The more recently designed steam headers, made from $\frac{1}{2}$ Cr– $\frac{1}{2}$ Mo– $\frac{1}{4}$ V class steel, make up the rest. On the basis

of current estimates 79 of these are due to be replaced before 2010 (Cane & Townsend, 1984). It can be seen from the pie chart and the accompanying figures that low-alloy ferritic steel steam headers are predominant in this list of problem steam headers, and as a consequence it is on these steels that the work in this project will focus, specific study being made of 1Cr- $\frac{1}{2}$ Mo type material.

1.5.2 Microstructure

It is known that in low-alloy ferritic steels the cementite is initially present either as relatively coarse lamellae in pearlite or as finer precipitates in tempered martensites and bainites, the latter case usually applying to steam boiler system materials (Wilson, 1986). The microstructure of header materials is commonly a mixture of allotriomorphic ferrite and bainite, formed by continuous cooling from austenite. The bainitic region is partially annealed during the fabrication process.

Bainitic carbides in these steels will be subject to coarsening during the high-temperature operation of the plant. The rate of such coarsening has long been known to increase greatly during creep (Jenkins & Mellor, 1942), and it is suggested that carbide coarsening could be used both to determine remanent life on a microstructural level and to develop a mechanistic creep damage model to improve remanent life assessment in the future (Wilson, 1986). The monitoring of microstructural development during service to develop a mechanistic model is a major aim of the work and is discussed fully in chapter four.

1.5.3 Operating conditions

The design operating temperature for fossil fuel boilers in UK power stations is typically about 568°C for 600MW plant, and about 540°C for 500MW plant, figures that are arrived at as a compromise between the increased efficiency and reduced service life associated with higher superheated steam temperatures. It has already been noted, however, that at certain times in problem areas (such as at the inlet tubes) this can be exceeded by some 40°C to 50°C. Operating temperatures at variance to design temperatures are found in two forms: irregular fluctuations during operation (figure 1.4), and spatial variations and the

development of problem ‘hot spots’ within a component (figure 1.4 and figure 1.5).

The operating temperatures for boiler systems with other fuel sources (*e.g.*, oil and gas fired power stations) are generally lower so that creep life exhaustion in the boiler system does not present such a problem (Cane & Townsend, 1984). Similar operating design temperatures are found in some nuclear installations outside the UK, but otherwise non-UK experience is similar (Wilson, 1986). Typical operating conditions in a 500MW fossil fuel power station are presented in table 1.2. The steam header regions in the boiler system of fossil fuel power stations, and in particular the critical areas noted, can therefore be expected to experience significant levels of creep during service.

Parameter	Typical value
Evaporation	$1.58 \times 10^6 \text{kg h}^{-1}$
Drum temperature	680°C
Drum pressure	18.3MPa
Superheater outlet temperature	541°C
Superheater outlet pressure	16.6MPa
Reheater inlet temperature	348°C
Reheater inlet pressure	4.3MPa
Reheater outlet temperature	541°C
Reheater outlet pressure	4.1MPa
Inlet feedwater inlet temperature	254°C

Table 1.2: Typical plant operating conditions

1.6 Current Remanent Life Assessment Procedures

The various procedures available to facilitate remanent life assessment can be considered to comprise two broad approaches.

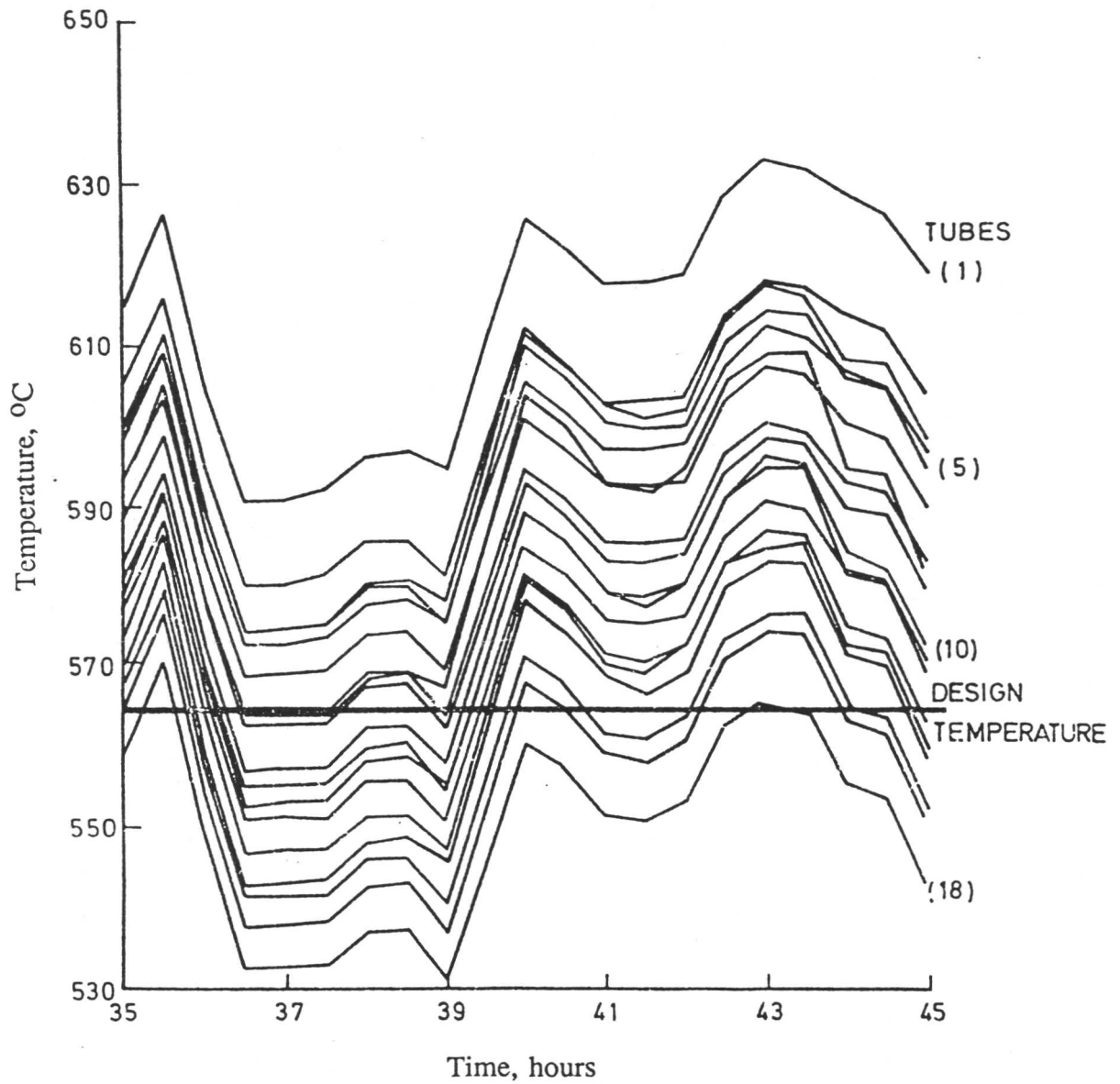


Figure 1.4: Inlet stub tube temperature variation around an eighteen tube element on a 500 MW reheater drum (from Cane & Townsend, 1984)

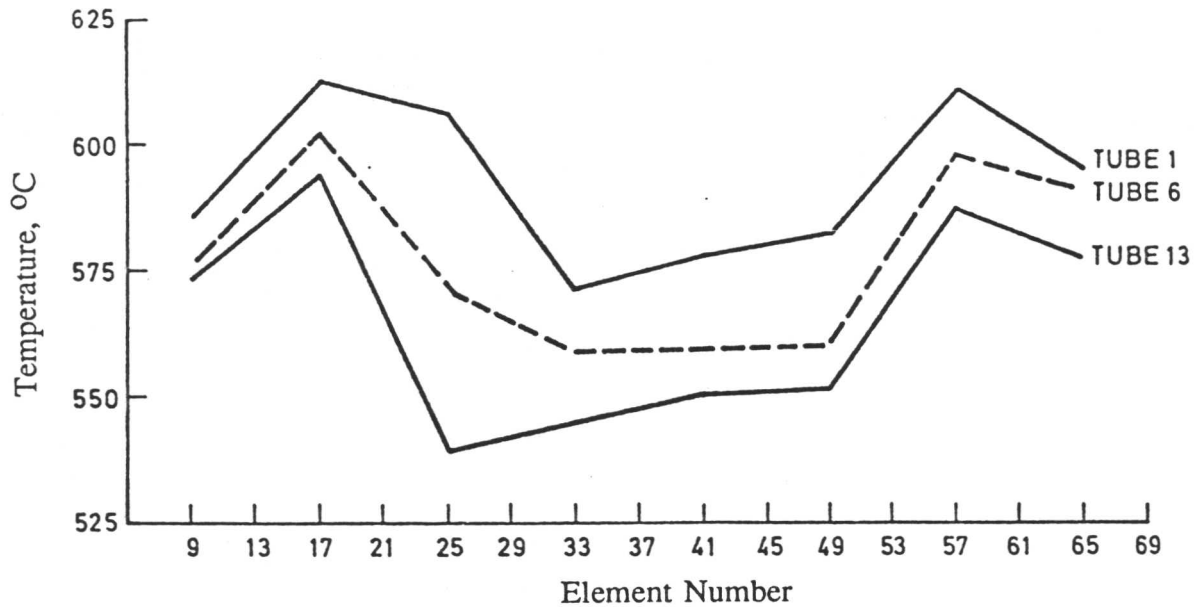


Figure 1.5: Reheater drum inlet stub tube temperature distribution in a 500 MW boiler (from Cane & Townsend, 1984)

- (a) Involves the monitoring of operational parameters (temperature, pressure, steam data *etc.*) and the use of the data collected in conjunction with standard materials data and the life fraction rule (below) in order to produce an estimate of available life for a component.
- (b) Examination of material which has seen service, in the form of external inspection of problem areas during service, and NDT and more detailed scrutiny during periods of plant outage. Crack detection, on plant strain measurement, and 'non-destructive' removal of small test specimens can all be carried out during periods of downtime. The test specimens can be used for post-service observations which could be microstructural, bulk physical (*e.g.*, crack examination) or mechanical (*e.g.*, accelerated creep rupture tests).

A practical life prediction programme will commonly include procedures of both types.

The approach that was adopted by the CEGB is given in a general operation memorandum “Creep Life Prediction of Headers” (CEGB, 1982), which divides the proposed procedure into three stages:

Stage I Based on measurements of steam temperature data, operational lifetime, minimum stress rupture data, design data and the life fraction rule.

Stage II An extension of Stage I but using dimensional checks rather than design dimensions, and measurement of actual metal temperatures.

Stage III Based on the use of test samples from service components and methods developed by the Remanent Life Task Force (to which this project is contributing).

Stages I and II follow an approach of category (a). They use established techniques that are known to give highly conservative estimates arising from the use of minimum stress rupture data and peak temperatures without allowing for stress redistribution; the inherent conservatism in design stress calculations compounds the error. These techniques are useful in identifying problem headers, however, where failure may be expected during the lifetime of the boiler system.

Stage III uses techniques developed by an approach of category (b) and it is hoped that models will be developed to overcome the inaccuracies of current procedures, thus allowing less conservative use of the headers.

1.7 Methods Based on Operational Data Monitoring

Data measurements are taken on the plant at regular intervals, in particular pressure and temperature (whence the creep strain on plant can be determined). These data are then processed using the ‘Life Fraction Rule’, the basis of which was originally proposed by Robinson (1952), namely:

$$\Sigma(t_i/t_{if}) = 1 \tag{1.1}$$

where t_i is the time spent at the stress, σ_i , and the temperature, T_i ; t_{if} is the failure time at σ_i , T_i . The rule assumes that linear summation of life fractions is possible, and recent work (see below) shows that this is not a satisfactory approximation in all situations.

1.7.1 Life fraction rule

The life fraction rule still forms the basis for beginning a remaining life analysis utilizing operational parameter measurements. However, investigations in the last decade have revealed limitations and the need for modification to the life fraction rule to fit particular circumstances.

Hart (1976) investigated the life fraction rule approach for both accelerated stress and accelerated temperature test procedures. This was done by subjecting pre-crept steel to accelerated rupture tests by both increasing temperature at original pressure and increasing pressure at original temperature. Hart discovered that summation of rupture life fractions arising from variations in temperature is more accurate than similar summation for variations in stress in the case of low-alloy ferritic steels; this is illustrated in figure 1.6 for 1Cr- $\frac{1}{2}$ Mo³ steel, comparing the observed residual lifetime after testing with a life fraction rule approach.

Work done by Hart (1977a) exposed a further problem with the life fraction rule approach. It was found that small test specimens which had been removed from a failed artefact (*i.e.*, life fraction consumed for the artefact = 1) retained a finite remanent life (*i.e.*, life fraction consumed < 1). It became clear that a greater understanding of the failure mechanisms would be necessary if these observed non-uniform damage distributions were to be accounted for.

Cane and Williams (1979) extended Hart's work, performing increased stress and increased temperature post-exposure simulations on Cr-Mo-V steels. They found that accelerated testing by increased temperature produced a re-

³ Exact compositions are frequently not given in the literature but will be quoted in footnotes where available. It should be borne in mind that when a composition is given as above Cr, Mo and V weight percentages are only approximate, C is in the approximate range 0.10-0.15 wt%, and other alloying elements (*i.e.*, Ni, Mn) are frequently present in these types of steel.

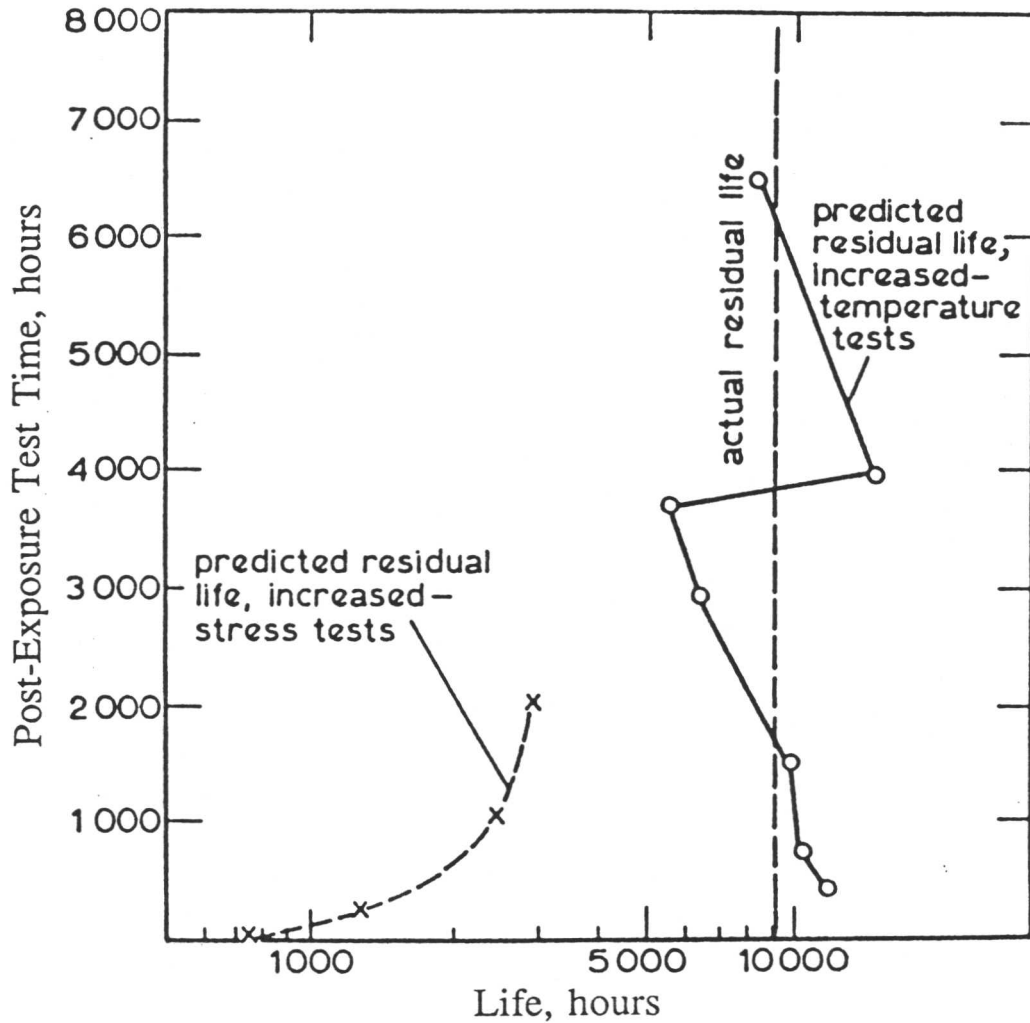


Figure 1.6: Life fraction rule life estimates for accelerated testing (from Hart, 1976)

maintaining life that was relatively insensitive to test duration, but that this was not the case for accelerated test procedures involving increased stress. This appeared to confirm the conclusion that for low alloy ferritic steel components a life fraction rule approach is a reasonable approximation where temperature varies markedly but not in cases where stress varies. It is proposed that these anomalies arise as a result of a recovery creep mechanism based on the creep damage processes proposed by Cane (1978). The general condition for validity

of the life fraction rule at all stresses, σ , and temperatures, T , is:

$$\frac{t_{tf_{\text{ex}}}(\sigma, T)}{t_{tf_{\text{unex}}}(\sigma, T)} = \text{constant} \quad (1.2)$$

where $t_{tf_{\text{ex}}}$ and $t_{tf_{\text{unex}}}$ are the failure times in tests on service-exposed and unexposed material respectively. Particle coarsening during service increases particle spacing within the microstructure compared with the pre-service material. Cane proposes that at high stresses a refinement or coarsening of the dislocation structure can occur much more freely, according to the recovery creep model, than is possible in the finer structure of the unexposed material; hence, accelerated testing by increased stress is sensitive to exposure time. At low stresses the mechanism is inhibited in both cases, and strain accumulation is governed by the resulting particle coarsening, so that test results do not show a sensitivity to exposure time.

The service conditions for steam headers will generally exhibit a much more severe variation in temperature than in steam pressure. As a result it can be concluded that for low alloy ferritic headers the limitations in the life fraction rule itself are unlikely to be of large import with respect to limitations in the accuracy of operational data measurements.

1.7.2 Errors arising during data processing

1.7.2.1 Variability in stress data

Limitations on determination of creep life from stress data are imposed by the difficulty in obtaining accurate measurements from in-service components; by variations between conditions and properties in different parts of the same cast; and by the complexity of the stress systems in components. The effect of scatter in stress data of up to 20% is shown in table 1.3 below, based on the stress to give failure in 100 000 hours in the case of $2\frac{1}{4}\text{Cr}-1\text{Mo}$ type steel for mean rupture data at 560°C (Cane & Townsend, 1984). Note that in table 1.3, zero stress represents the mean stress and -20% and $+20\%$ correspond to lower and upper bound limits respectively; the lower bound (-20%) data thus correspond

% Change in stress	-20%	-10%	-5%	0	5%	10%	20%
Failure time, hours	38 000	62 000	78 000	100 000	110 000	130 000	200 000

Table 1.3: Effect of stress variation on creep life

to an increase in the stress experienced by the test piece, and a reduction in the time to rupture.

A normal level for bounding accuracy limits in this sort of data analysis is 10% or 20% (Price & Williams, 1982) and for safety reasons the lower bound for rupture life must be used. As most measured data presently available cover only the first half of the planned operational lifetime the necessary conservatism is compounded further, so that underestimation in rupture life using such a lower bound approach could be as great as five times the actual life (Cane & Townsend, 1984).

In addition, there is an absence of significant quantities of data from fundamental investigations into the physical metallurgy of these steels; in particular, the exact chemical and microstructural composition of an individual batch of steam headers is unlikely to be known. This forces the researcher to repeat the fabrication heat treatments on service material in order to reproduce the initial microstructure before work can proceed. The reproducibility of results from such a procedure can not be guaranteed in all cases; for example, Stevens and Flewitt (1984), working with creep resistant steel Durehete 1250, found it impossible to create the initial condition by simulating the fabrication processes. This type of case is unusual, and in the absence of archive material a regenerated material procedure is normally satisfactory, but the work by Stevens and Flewitt illustrates the care which must be employed.

1.7.2.2 Errors in data extrapolation procedure

The procedures involved in extrapolating and applying standard material data

from small test specimens to $1-2 \times 10^5$ hours and thick-section material are complex. In particular, the effect of oxidation on the lifetime obtained from test specimens has been found to be significant by several workers; a comparison of creep curves for air and vacuum is shown in figure 1.7. It is clearly illustrated that an appreciable reduction in the lifetime of a test specimen when tested in air is exhibited, compared with similar testing in a vacuum; and hence, full consideration of comparative environmental factors is essential if test results are to be extrapolated to real systems.

The effect of environmental conditions on test piece lifetimes gives rise to a further complication: the creep lifetime of small test pieces can be expected to show a strong dependence on the section thickness of the test piece, as has been shown experimentally (figure 1.8). This effect is attributable to several causes: the reduction in actual metal cross-section, which occurs during creep testing as a result of oxidation, produces a non-load-bearing surface oxide layer, a process known as oxide weakening (Shahinian & Achter, 1963); surface properties may be altered by decarburization (Borgreen & Huntley, 1984); and, in some cases, a compact, partially-load-bearing film can form on the surface, leading to an increase in creep life, a process referred to as oxide strengthening (which is effectively the opposite to oxide weakening) (Shahinian and Achter, 1965). Both oxidation and decarburization effects can be exaggerated by grain boundary penetration near the surface. All the above are surface effects, so can be expected to exert a greater influence on a specimen with a higher surface:volume ratio (*i.e.*, for a smaller diameter test piece); therefore, standard data from small specimens tested in air may significantly underestimate the rupture life of thick-section material if extrapolated directly. If reasonably representative results are to be produced by post-service testing, it will frequently prove necessary that they be carried out in an inert environment, as discussed later. Nevertheless, the above factors render any attempt to extrapolate standard small cross-section test piece data to thick-section material in a moderately corrosive environment (in the sense that the component is at elevated temperature and exposed to the weather) difficult to carry out with confidence; hence the necessity of large

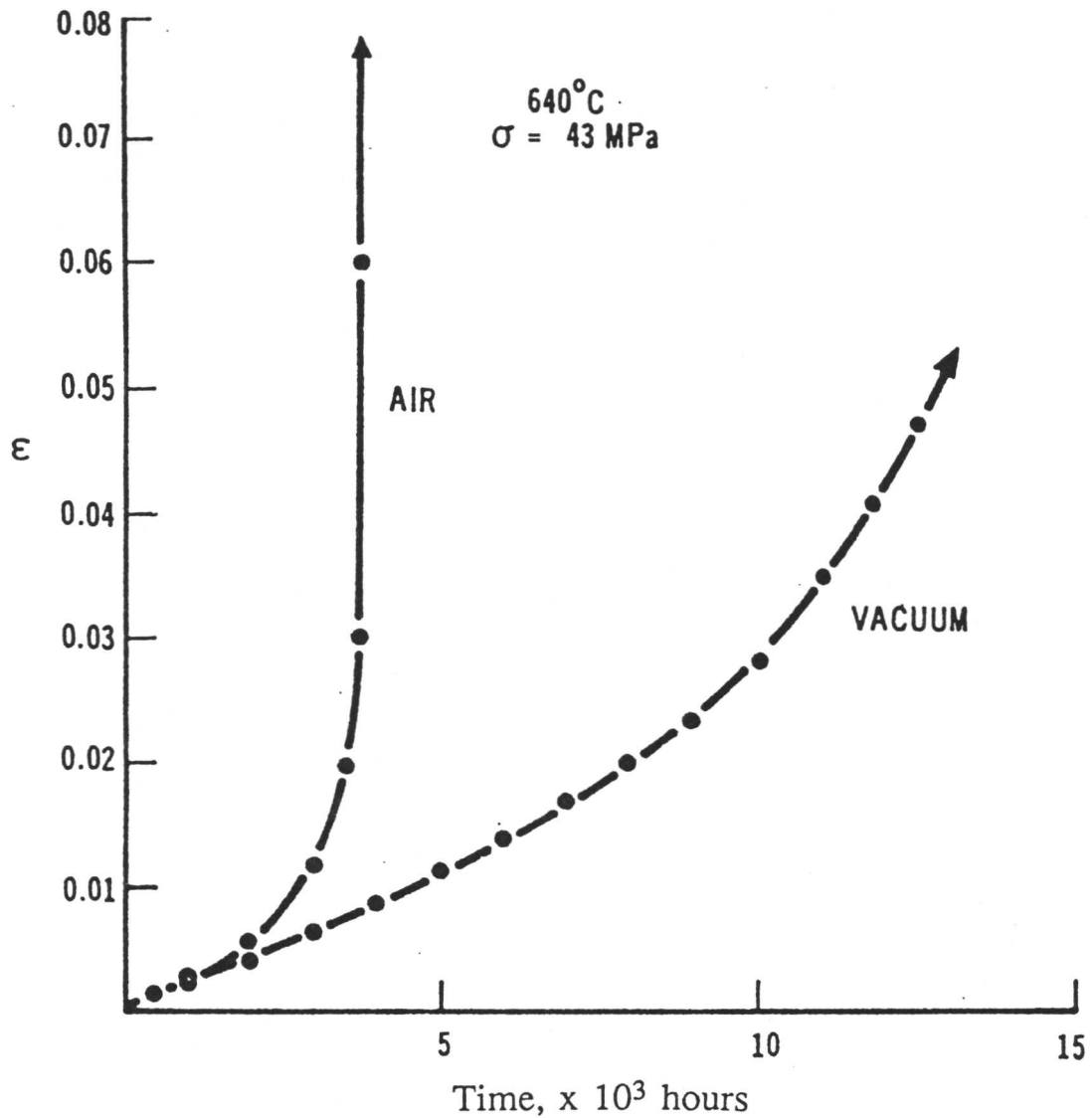


Figure 1.7: Creep curves for Cr-Mo-V steels in air and vacuum (from Cane & Townsend, 1984)

safety factors to accommodate this inevitable uncertainty, which could lead to a design life being substantively less than the true creep life of the component.

1.7.2.3 Choice of representative stress

Standard data are generated under uniaxial conditions, whereas components in service are subject to highly-complex stress systems associated with the multi-

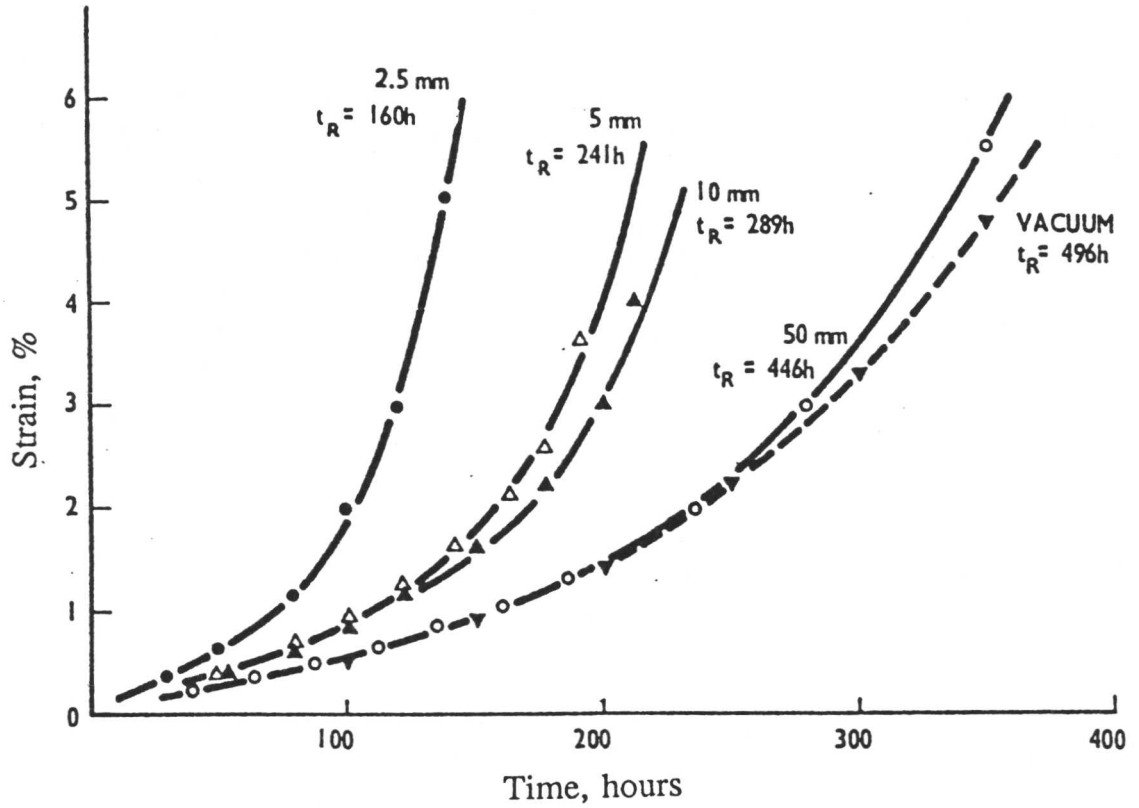


Figure 1.8: Creep curves for various test piece diameters tested in air

axial loading conditions. It becomes necessary to use a representative stress, a semi-empirical approximation to the real stress system, which is usually referred to as either σ_{ref} or σ_r , to characterize the complex system to a simple case for which standard test data exists. A simple but widely-used example of a practical representative stress is the mean diameter hoop stress (MDHS):

$$\sigma_{\text{ref}} = \frac{P(d_0 - t)}{2t} \quad (1.3)$$

where d_0 is the outer diameter, t is the wall thickness, and P is the pressure. This is referred to as an example only: various other representative stresses have also been proposed as applicable for different situations, but a detailed discussion of this method is outside the scope of this work. It should be noted, however, that any representative stress is intrinsically an empirical approximation, necessitated by the impracticability of modelling the true stress system, and work by

Cane and Brown (1982) found the true reference stress to be significantly lower than the MDHS. When the problem of accurately determining exact dimensions during the deformation process is considered (dimensions are generally taken from the design specifications to a first approximation, but will, in reality, vary by some finite amount as creep strain is accumulated during service). It has been suggested that the use of MDHS as a reference stress may overestimate the actual stress by as much as 20%; this has been shown to correspond to a lifetime underestimate by a factor of two (Cane & Townsend, 1984).

1.7.2.4 Temperature

Errors can arise from spatial variations of steam temperature within the header, irregular fluctuations of operating temperature, and instrumental imprecision. The effect of variation in temperature on rupture life is shown in table 1.4, based on a mean stress to failure in $2\frac{1}{4}\text{Cr}-1\text{Mo}$ steel at 560°C in 100 000 hours; a variation of just 10°C being found to corresponds to a factor of two difference in the resulting rupture life estimate (Cane & Townsend, 1984).

Temperature, $^\circ\text{C}$	540	550	560	570	580
Failure time, hours	250 000	170 000	100 000	56 000	32 000

Table 1.4: Effect of temperature variations on creep life

1.7.3 Summary

The problems associated with a remanent life prediction procedure based on standard data and the life fraction rule are well documented. As a result, the CEGB programme outlined in GOM101A (CEGB, 1982), and continued by National Power PLC, concentrates on post-service testing as the most probable way in which the accuracy of the assessment procedure can be improved. Operation data methods are envisaged to play an increasingly secondary role, that of iden-

tification of problem areas that should be subjected to a fuller analysis of the stage III type.

1.8 Methods Using Post-Service Material

Sampling of materials from components that have been in service can be utilized either for testing of mechanical properties or for direct assessment of the remaining life from the microstructural state. In both cases it is necessary to develop models of the processes involved in creep damage in order to determine the remaining life from the metallographic feature or bulk property under observation (Cane, 1983).

1.8.1 Creep damage models

There are two basic approaches to creep damage modelling: mechanistic and parametric modelling. Mechanistic modelling is to be preferred as service conditions can be related to microstructural changes and thus to creep damage directly. Parametric models are largely empirical models which have been found in the past to give reasonable creep life predictions from operational data in certain situations, but which are not fundamentally related to any considerations of creep damage processes. The combination of the limited theoretical basis of parametric models, and the difficulties in collecting and interpreting operational data outlined above, limits the accuracy of life prediction on the basis of parametric creep damage models. At present, however, development of good mechanistic models is far from complete so in practical situations parametric modelling is used.

1.8.1.1 Damage processes

For low-alloy steels four processes are of relevance:

- (i) Creep strain accumulation without significant decrease in creep strength. This occurs in cavitation resistant microstructurally-stable materials, the onset of failure being governed by reduction in section and corresponding increase in net section stress with increased strain rate (Cane & Williams, 1987).

- (ii) Microstructural degradation (*e.g.*, precipitate coarsening, modification of the dislocation mesh structure by the increase in interparticle spacing) leading to a continuous reduction in creep strength during service.
- (iii) Creep cavitation, which is usually observed at grain boundaries.
- (iv) Environmental attack (external scaling, internal oxidation or decarburization *etc.*).

The four processes occur simultaneously, but depending on materials and conditions one or other will predominate. Processes (ii) and (iii) are creep damage processes which will enhance the rate of increase of the strain rate until tertiary creep and failure can take place; these are of particular significance for the high-temperature failure of low-alloy ferritic steel plant. In general, coarsely-microstructured materials such as weldments are susceptible to cavitation damage, whereas in the more refined microstructure of the bulk boiler steel ductile damage processes are favoured (Cane & Townsend, 1984). Thus for steam header bodies, where, as noted earlier, improvements in current predictive techniques could be of greatest value, mechanism (ii) is of most relevance.

1.8.1.2 Mechanistic creep damage model for headers

Initially, the role of cavitation can be ignored as its contribution to header failure is small. If the dominant ductile mode of failure is then considered we can model low alloy ferritic steels as particle dispersion hardened material with a creep rate primarily dependent on particle spacing (Cane & Williams, 1987). In developing such a model it is necessary to consider:

- (a) An exact relationship between creep rate and particle spacing, which will require an understanding of the mechanism by which dislocations overcome particles to move through the matrix (Cane & Townsend, 1984).
- (b) An accurate description of the variations in particle dispersion in different regions of the material.
- (c) An understanding of the effect of time spent at elevated temperature and pressure on particle dispersion and size.

(d) Solid solution strengthening.

It is on this basis that attempts can be made to determine the creep rate from the operating conditions and thus estimate creep life. Ultimately, models of this basic design show great potential for improving the accuracy of remanent life estimates, but at present they are very much in the development stage.

1.8.1.3 Parametric creep damage model for steam headers

These models have been available for some time, developing from a continuum approach to the analysis of tertiary creep by Kachanov (1958) and others. The concept of a damage parameter, ω (a scalar quantity which is zero at the start of exposure and one at the point of failure), is introduced to give a quantified level to the creep damage and thus to the remanent life. Damage and strain are assumed in Kachanov's approach to increase as functions of stress and temperature.

Using such an approach leads to a relationship such as the one below, proposed by Rabotnov in 1969, to relate the strain rate, $\dot{\epsilon}$, and the rate of creep damage accumulation (*i.e.*, the rate of change of the creep damage parameter with respect to time), $\dot{\omega}$, to the stress state. It is presented as an example of a parametric model: a full discussion of models in current use in the Industry is beyond the scope of this summary.

$$\dot{\epsilon} = \frac{A \sigma^n}{(1 - \omega)^n} \quad (1.4)$$

$$\dot{\omega} = \frac{B \omega^\nu}{(1 - \omega)^\eta} \quad (1.5)$$

The relationship is essentially empirical, with A, B, n , η , ν , and σ being constants characteristic of the material; thus it follows that such a model requires quantities of archive test data if it is to be established, and the problems associated with determining accurate test data and operational parameters are well documented above. As a result, although a parametric model provides a reasonable basis from which to make an assessment of remaining life, a mechanistic model would be preferable.

1.8.2 Mechanical testing

1.8.2.1 Accelerated creep and rupture tests

Testing is carried out under accelerated conditions (of increased stress, temperature or both) on material taken from service, which has partially exhausted its theoretical creep life. Rupture testing involves simply the determination of time to rupture for varying simulation conditions, whereas creep testing assesses the strain response of the material as the simulation proceeds. Generally, only small pieces of material are taken for testing, but in extreme cases whole components are used (Day, Rowley & Williams, 1979).

1.8.2.2 Rupture testing

For thick walled components, such as steam headers, rupture testing is typically carried out using samples under uniaxial stress with a specimen axis parallel to the maximum principle stress direction of the component (Cane & Williams, 1979). One or other of the approaches below can then be used to determine residual life from time to test piece rupture.

(a) Parametric extrapolation

There are two general experimental techniques which allow creep life assessment to be made within reasonable periods of time, involving accelerating creep rate by changing the conditions. These accelerated tests have the disadvantage that the results have to be extrapolated to the slower strain rates associated with service conditions. The first of these, stress extrapolation, employs isothermal rupture tests performed over a range of temperatures at stresses above the nominal service stress. The extrapolation of increased stress conditions to the lower service stress is based on largely-empirical relationships which do not take account of mechanistic considerations, such as the recovery mechanism proposed by Cane (1978, see Section 1.7.1); however, it has been observed experimentally that remanent life predictions based on stress extrapolation tend to be optimistic (Cane & Townsend, 1984), so the technique has limited engineering value.

Testing in accelerated conditions achieved by raising the temperature at the nominal service stress are also carried out (temperature extrapolation). Hart (1976), Cane and Williams (1979) and others have all proposed that this is a more satisfactory method than stress extrapolation for low-alloy ferritic steels: work carried out by Hart (1980) for Cr–Mo–V samples removed after 100 000 hours service gave an extrapolated service life of 150 000 hours at 571°C, compared with the figure in excess of 200 000 obtained from stress extrapolation experiments; and experience gained from components in service suggests that the former is almost certainly a more reliable estimate.

An understanding of this observation can be achieved by considering the mechanistic applicability of accelerated testing methods. It has been observed that microstructural damage (carbide coarsening *etc.*) rather than void formation is the predominant damage mode found in practice in steam headers. At low stresses, precipitate coarsening controls the development of the dislocation structure and the distribution and movement of dislocations within the microstructure; precipitate coarsening (and the concomitant increase in interparticle spacing) will thus govern the deformation rate. At higher stresses, the dislocation mesh size will decrease until it becomes less than the interparticle spacing; dislocation movement will then cease to be governed by the precipitate dispersion, and the dislocation structure can modify allowing some recovery to take place. Consequently, the rupture life becomes highly stress sensitive, and extrapolation wildly inaccurate, as is illustrated schematically in figure 1.9.

Temperature extrapolation can then be expected to be a superior procedure provided no fundamental changes in the nature of the precipitates occur: any change in the properties of the carbides could be expected to affect the creep behaviour and introduce a temperature sensitivity. It should be noted that observations by Felix and Geiger (1961) suggested that for Cr–Mo–V steel such a change did occur, (from VC to Mo₂C at 600°C), showing that this difficulty is encountered in engineering systems, so care must be taken to monitor carbide structure if temperature extrapolation is to be carried out.

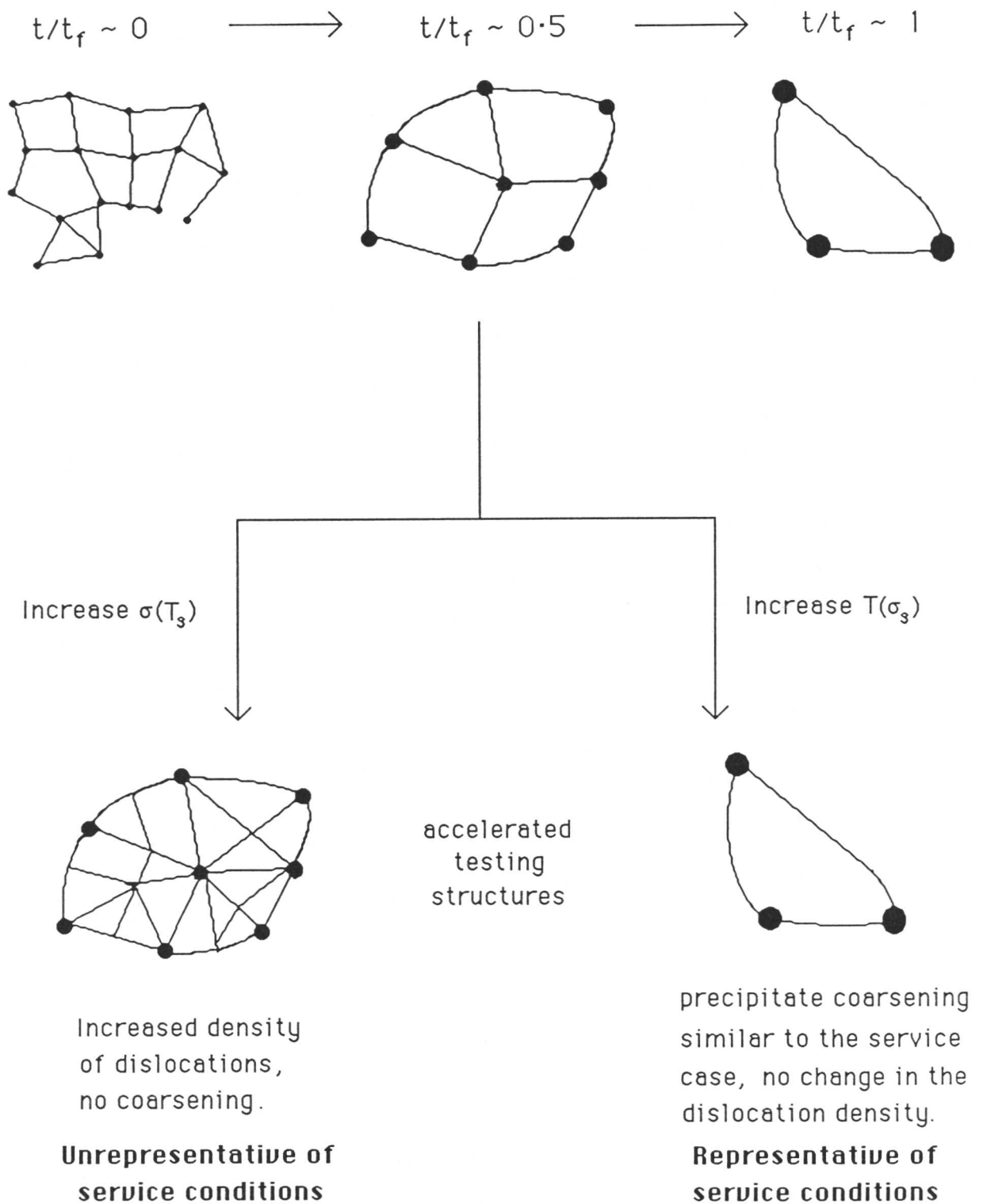


Figure 1.9: Structural aspects of accelerated rupture test methods (Cane & Townsend, 1984)

(b) Life fraction rule

The life fraction rule (equation (1.1)) can be simplified for accelerated testing, to:

$$\frac{t_s}{t_{sf}} + \frac{t_t}{t_{tf}} = 1 \quad (1.6)$$

where t_s is the time at service conditions, t_{sf} is failure time at those conditions, and t_t and t_{tf} represent the corresponding times for test conditions.

The application of the life fraction rule was discussed in Section 1.7.1, and it was noted that it is generally more applicable to accelerated temperature tests for low-alloy ferritic steel (see, for example, Hart, 1977a,b): stress acceleration is only acceptable where the creep strength has not been affected by unstressed thermal exposure (Hart, 1980). The disadvantage with a life fraction rule method is the general shortage of virgin material data (to provide t_{tf}). Thus t_{tf} must frequently be based on estimates from lower bound stress test data or from tests on regenerated material with the inherent inaccuracies that introduces (Cane & Williams, 1985).

1.8.2.3 Creep testing

(a) Constant strain rate

Material is tested under laboratory conditions at a constant, but considerably higher than service, secondary creep strain rate. This involves the extrapolation of data obtained at the high laboratory strain rates to the lower rates experienced in service, hence the same problems are encountered as those noted for high-stress rupture testing (above) (Cane & Townsend, 1984).

(b) Constant load

Testing is carried out at the service stress and the creep strain rate is increased by increasing the temperature to considerably above the service temperature. Minimum creep rate ($\dot{\epsilon}_m$) in post-exposure tests over a range of temperatures is extrapolated on a $T - \dot{\epsilon}_m$ plot to obtain the creep strain rate expected at the

service conditions. Cane (1982) and others have found that this approach, which depends on creep rupture and creep deformation having similar mechanisms, gives reasonable accuracy for low-alloy ferritic steels.

1.8.2.4 Other mechanical tests

Techniques can also be developed to relate a measured bulk physical property to the creep life; such a property must of necessity show a known correspondence to the relevant creep mechanism. Those methods which have been found useful are listed in table 1.5 (Cane & Townsend, 1984).

Test Method	Comments
Tensile	Limited applicability
Charpy V notch	Limited applicability
Hardness	Useful as a non-destructive method to isolate problem areas
Low cycle fatigue	Insensitive to structural damage, not generally applicable
Hot tensile	Sensitive to structural damage but not directly relatable to remanent life
Internal friction	Research tool only. No advantage over accelerated creep testing (see above)
Density, resistivity, magnetic permeability, small angle neutron scattering	May be useful for cavitation assessment in microstructurally-stable material

Table 1.5: Applicability of mechanical testing to the determination of remanent creep life

1.8.3 Metallographic examination

Metallographic studies, based on the models developed for creep damage (Cane, 1978), can potentially be used to estimate remanent creep life from small samples

of material taken from the exposed component. The technique has the advantage of being essentially non-destructive: samples can be taken by removing small slices, cylinders or cones of material from the critical region (which can then be repaired), or by acetate surface replica methods (Townsend, 1986), without damaging the bulk material.

Properties that can be studied include carbide size, spacing, composition and type, and local void distribution (Cane, 1984). Any carbide assessment will be via SEM or TEM procedures on post-service material, but the use of surface replication is efficacious in studying distributions of voids and microcracks (Cane & Williams, 1987). If this approach is to be practicable, it is imperative that a correspondence between remanent life and a given level of microstructural damage be established. Of the properties listed in the table, the level of cavitation, or fraction of cavitating boundaries, have been proposed as the most suitable expressions to appertain to remanent life (Cane & Needham, 1983), as is illustrated for the heat affected zone of a $2\frac{1}{4}\text{Cr}-1\text{Mo}$ type steel in simulated laboratory conditions in figure 1.10. It must be noted, however, that a given degree of cavitation could represent very different consumed life fractions for different stress states: Ludwigsen (1985) observed 0.1% cavity area as corresponding to 30%–70% damage, so that only qualitative lifetime judgements could realistically be made on such observations of the extent of cavitation. It will be necessary for genuinely representative mechanistic models to be developed before metallographic techniques can reach a high level of sensitivity.

At present, only surface replica techniques are used frequently, as they have the advantage of giving a warning of serious creep damage at critical areas cheaply and quickly and without requiring a knowledge of the thermal history of the component (Vierros, 1985). Nevertheless, metallography is of value both at present, as a preliminary NDT technique to isolate critical areas for creep life exhaustion, and as an experimental route to the development of mechanistic models.

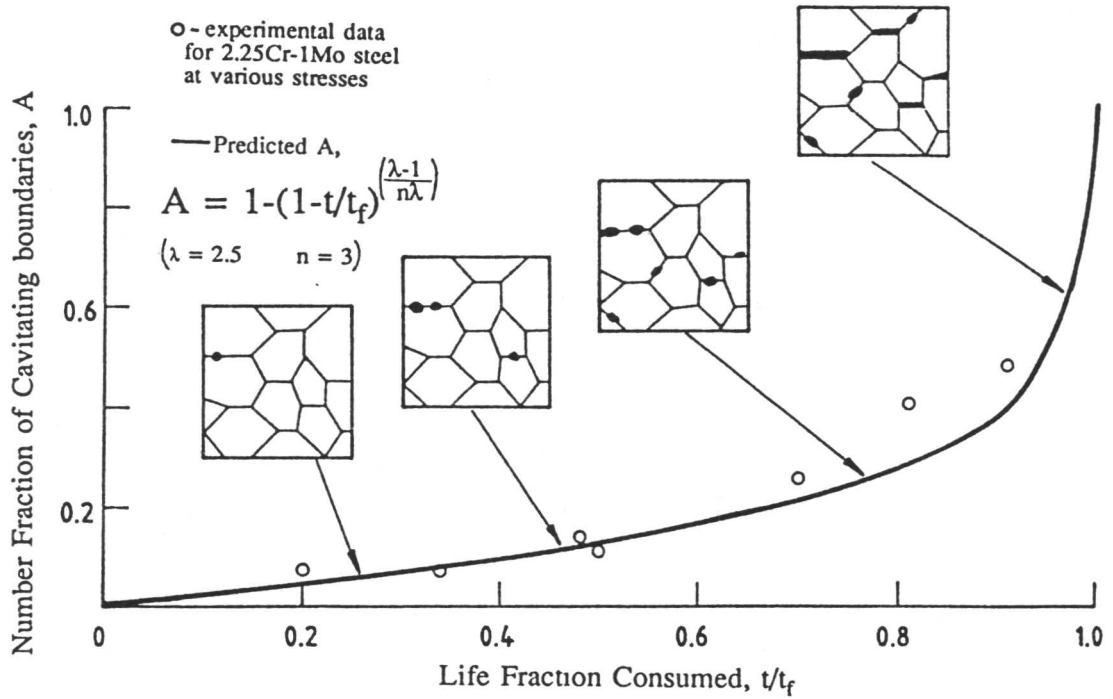


Figure 1.10: Relationship between fraction of grain boundaries showing signs of cavitation and life fraction consumed (Cane & Townsend, 1984)

Chapter 2

MICROSTRUCTURE OF CREEP RESISTANT LOW-ALLOY FERRITIC STEELS

The principal influence on development of steam header material is provided by the heat treatments that are performed to transform from austenite to ferrite, and to modify the ferritic microstructure to produce the desired properties in the final product. Nevertheless, the solidification processes effecting the production of the initial cast are of importance, as solidification induced segregation within it could have a significant effect on the development of ferrite from austenite during steam header fabrication. In this context the effect of alloying element segregation on the austenite–ferrite transformation must also be considered.

2.1 The Austenite–Ferrite Transformation

The decomposition during cooling of the higher temperature face-centred-cubic γ -iron structure to the less dense body-centred-cubic allotrope (α) gives rise to a variety of different morphologies and microstructures, depending on the cooling rate, presence of alloying elements, conditions and availability of lower-energy nucleation sites for heterogeneous nucleation.

2.1.1 *Effect of cooling rate*

Increases in undercooling and rate of cooling from the austenite region limit the ability of alloying elements in iron, and the iron atoms themselves, to diffuse during the transformation to form the equilibrium structure, hence leading to an increased tendency for the formation of metastable structures.

The alloying elements in steel can be categorized in two classes. Substitutional elements (*e.g.*, Cr, Mo) occupy lattice sites within the iron lattice and require vacant lattice sites to facilitate diffusion. Hence these species are slow diffusers, which can only maintain equilibrium at the higher transformation temperatures; the same applies to the iron atoms. Interstitial elements (*e.g.*, C) are

fast diffusers, occupying and moving between interstices within the iron lattice. Diffusion of these species is suppressed only at much higher undercoolings. Whether the reaction process and rate is under the control of one or other type of diffusing species, or is diffusionless, is determined by the free energy for the transformation (which increases with undercooling) and by the diffusion rates (decreased with temperature); hence, cooling rate is critical in determining the transformation process, and consequently the final microstructural development.

2.1.2 Summary of transformation products

2.1.2.1 Allotriomorphic ferrite (α)

At low undercoolings, given sufficient substitutional atom mobility, the fcc lattice can undergo a reconstructive transformation to the bcc form via diffusional motion of the atoms. This is possible even without the maintenance of equilibrium concentrations of alloying elements throughout the structure; indeed, in the low-alloy ferritic steels typically used in power plant construction, at all but the slowest growth rates, reconstructive transformation is generally found to occur as a carbon-diffusion-controlled growth process with no bulk partitioning of substitutional alloying elements, via a para-equilibrium mechanism suggested by Hillert (1952).

Diffusional ferrite in steels is generally found to nucleate heterogeneously and is observed to grow into two forms, allotriomorphic and idiomorphic. Allotriomorphic ferrite is the term applied to ferrite regions where the crystal structure and symmetry is not directly reflected in the shape of the bulk region, whereas in the case of idiomorphic ferrite the ferrite region has a shape which corresponds to the crystal structure (Bhadeshia, 1985). The difference arises from varying growth processes for different nucleation sites.

Allotriomorphic ferrite nucleates at prior-austenite grain boundaries, and its morphology arises from the fact that the grain boundary provides a favourable growth path, so that the ferrite grows at a preferential rate along the boundary compared with other directions. In general, it has been shown that the growth of ferrite allotriomorphs is a diffusion-controlled process (Atkinson *et al.*, 1973).

A reproducible orientation relationship is often shown between the ferrite and one of the adjacent austenite grains, and in consequence it has been proposed that transformation proceeds by a route which involves ferrite nuclei forming a partially-coherent interface with one austenite grain, and an incoherent one with the other (Smith, 1953). The former (lower energy) interface then moves via a ledge displacement mechanism, with the latter (high-energy) interface being displaced by a continuous motion of the whole. However, it has been demonstrated that a ferrite nucleus can by chance exhibit such an orientation relationship with both the austenite grains at whose interface it forms (Hillert, 1962). The ledge-type growth mechanism is believed to play a significant rôle in the precipitation mechanism for certain of the alloy carbide structures that were noted earlier to be implicated in creep strength processes in low-alloy ferritic steels (Edmonds & Honeycombe, 1978).

In alloy steels, a variety of mechanisms of allotriomorphic ferrite formation are shown at different levels of undercooling below the $\alpha / \alpha + \gamma$ phase boundaries, which are governed by the partitioning behaviour of the substitutionals. Only at slow growth rates, at undercoolings marginally below Ae_3 , will the extent of partitioning of alloying elements between the phases be that predicted by an equilibrium tie line construction through the mean alloy composition: at higher undercoolings, the transformation proceeds via a partitioning local equilibrium (PLE), negligible partitioning local equilibrium (NPLE), or paraequilibrium (ParaE) mechanism.

These mechanisms where full long range equilibrium is not maintained can be explained by the large difference in diffusivity between substitutional and interstitial alloying elements, coupled with the need to maintain a mass balance for both species across the moving interface. It can be considered that, for diffusion-controlled growth, the alloying element compositions at the growth interface should approximate to equilibrium, even at growth rates where long range equilibrium cannot be maintained (Darken & Gurry, 1953). At low undercoolings, where the driving force for growth is relatively small, reasonable levels of diffusion are possible within the austenite at the interface. The diffusion fields

at the interface are such as to allow a large degree of partitioning of alloying elements at the growth front, hence the mechanism is termed partitioning local equilibrium (PLE).

At higher undercoolings and supersaturations the driving force for interface motion is increased, reducing the extent to which long range diffusion of substitutional alloying elements can occur during growth. The composition profile of substitutionals at the interface becomes narrowed to an increasingly pronounced spike, and the extent of partitioning at the interface becomes extremely small, leading to the process being labelled negligible partitioning local equilibrium (NPLE).

It should be noted that for both local equilibrium mechanisms motion of the interface is controlled by alloying element diffusion, even where partitioning of that element is negligible. This need not be true at higher undercoolings, where the driving force for motion of the interface can be sufficiently high to cause local equilibrium to break down, with insufficient time even for the small amount of longer range diffusion which is essential to a local equilibrium mechanism. Under these conditions the alloying element is configurationally frozen, and growth of the interface is controlled solely by diffusion of carbon, which reaches equality of chemical potential subject to the constraint that the Fe:X ratio is constant everywhere. This mechanism is referred to as paraequilibrium (ParaE). It may be remarked that a ParaE growth mechanism results in identical concentrations of alloying elements in α and γ_{ret} in a partially-transformed specimen, a feature which has been employed producing some of the microstructures used in this piece of work, where accurate knowledge of starting compositions was required.

2.1.2.2 Idiomorphic ferrite

Nucleation of idiomorphic ferrite takes place intragranularly at point sites (*e.g.*, inclusions), so that no preferential growth direction exists; in consequence, the crystal symmetry of the ferrite is reflected in the morphology of the bulk structure. In steels, idiomorphic ferrite generally takes the form of equiaxed grains (see, for example, Bhadeshia, 1985).

2.1.2.3 Widmanstätten ferrite (α_w)

At slightly higher undercoolings not far below Ae_3 temperature the increased free energy driving force for the reaction and decreased atomic mobility leads to the formation of Widmanstätten ferrite. The transformed region of this reaction product is found to be plate-shaped, with a thin wedge section, and an associated shape change (Watson & McDougall, 1973). A single Widmanstätten ferrite wedge is found to exhibit a shape change consisting of two adjacent and opposite invariant plane strains with a large (~ 0.4) shear component (Bhadeshia, 1981a). This lends support to the hypothesis that atomic correspondence for substitutional atoms and iron is maintained during the formation of α_w from austenite.

The strain energy that is associated with such a shape change has been determined from strain and elasticity data and measurements of aspect ratios (Bhadeshia, 1981a), and is found to be much larger than could be sustained by the available driving force. If a plate is to form this strain energy must be dissipated during the transformation. Widmanstätten ferrite formation becomes possible because the strain energy is largely accommodated by a growth process involving cooperative development of two mutually-accommodating plates into a characteristically wedge-shaped region of α_w , as shown on figure 2.1. Both of the plates are found to exhibit a KS-NW type orientation relationship with the initial austenite (Bhadeshia, 1981a).

As Widmanstätten ferrite forms at relatively low undercoolings, diffusion of carbon occurs during growth; in fact, the growth rate has been shown to be determined by carbon diffusion rates at the (glissile) α_w/γ reaction interface (Bhadeshia, 1981a).

2.1.2.4 Bainite (α_b)

At higher undercoolings bainite forms in sheaves originating from austenite grain boundaries. The transformed region exhibits an IPS with associated shear component of 0.22. In the absence of the cooperative growth process the associated strain energy is considerably higher than was the case for α_w . This is coun-

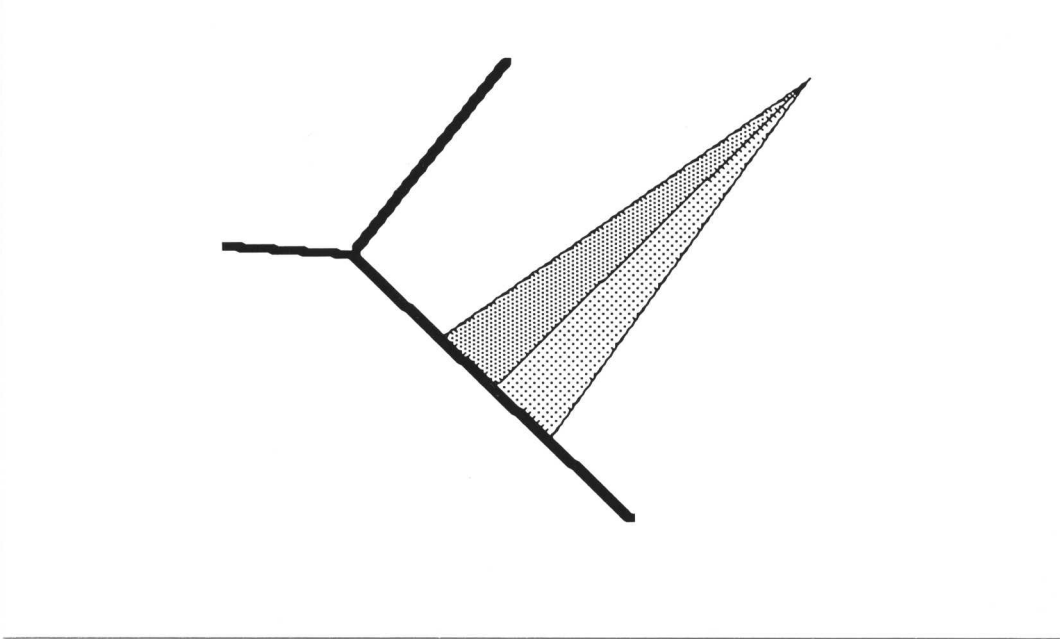


Figure 2.1: the back-to-back arrangement of plates of Widmanstätten ferrite growing from prior-austenite grain boundaries, illustrating the characteristic wedge shape of a Widmanstätten ferrite region

terbalanced by the increased free energy driving force which exists at the lower transformation temperature (Bhadeshia & Edmonds, 1980). This transformation product has been of great significance in the work outlined in this dissertation, and consequently the bainite transformation is considered in detail in a later section.

2.1.2.5 Martensite (α')

At highest undercoolings and low temperatures, where the free energy change for transformation is very large, martensite forms. The product arises as a result of a diffusionless transformation with direct atomic correspondence between parent and product lattices. There is macroscopically an IPS shape change in the transformed region giving rise to very large stored strain energy within the product phase; consequently, it is only able to form at high undercoolings where the chemical free energy change is large enough to offset this (Bhadeshia, 1985).

2.1.3 The time-temperature-transformation diagram

The concept of a time-temperature-transformation (TTT) diagram can be introduced to represent schematically the nature of transformation products and rates of reaction for different isothermal transformation temperatures in a given steel (*e.g.*, figure 2.2). Development of an accurate diagram of this sort for a particular alloy composition enables heat treatments to be designed to produce a desired transformation product.

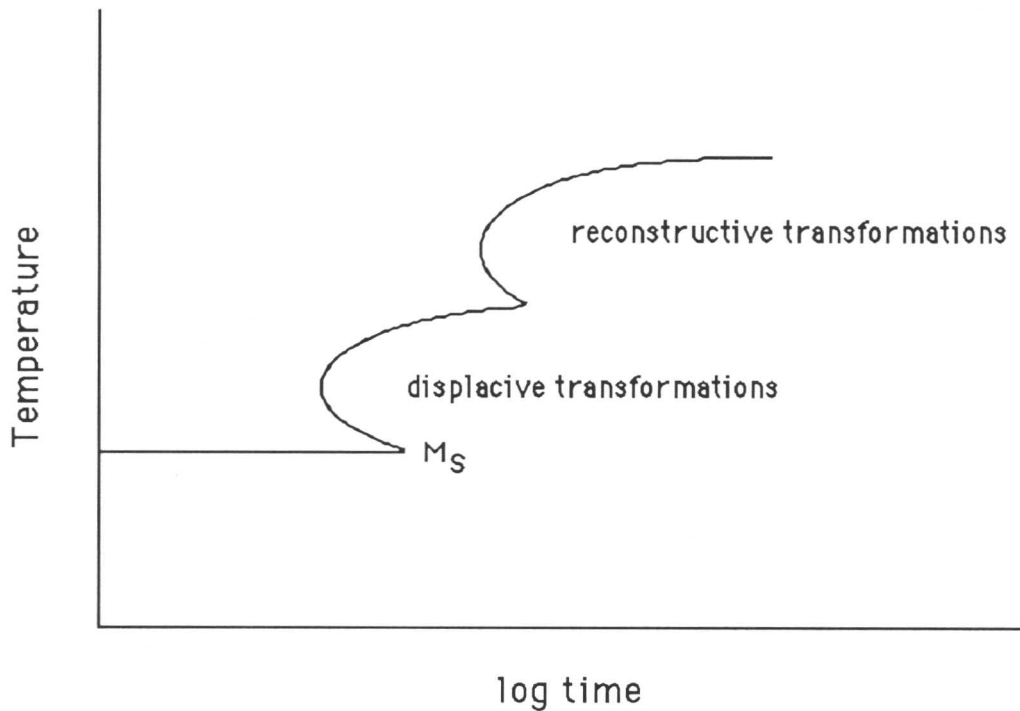


Figure 2.2: Typical TTT diagram for a low-alloy steel

2.1.4 The case of power station creep resistant steels

As we have noted for power station boiler systems the sequence of heat treatments is designed to produce a microstructure of allotriomorphic ferrite and bainite (α_b being in the range of 0.2–0.8 by volume fraction, usually around

0.2 for 1Cr- $\frac{1}{2}$ Mo type steels) (Cane & Townsend, 1986). Studies in this project have concentrated on determining remanent life from the appearance and ageing behaviour of the bainitic regions and alloy carbides found within the allotriomorphic ferrite, so a deeper consideration of these microstructural features is given below.

2.2 The Bainite Transformation

Bainite forms from austenite in steels in the temperature range below temperatures at which pearlite forms, and above the martensite start temperature. It consists of a non-lamellar aggregate of roughly lath or plate shaped ferrite grains, with carbide precipitation between and also sometimes within the ferrite. The bainite transformation has presented difficulties in interpretation, and remains the subject of some controversy.

2.2.1 Microstructural features of the transformation

Bainitic ferrite platelets or laths are observed to accumulate into sheaves possessing a roughly wedge-shaped morphology, and apparently originating from prior-austenite grain boundaries (Bhadeshia, 1988). The growth of these bainite sheaves is found to be limited by hard impingement with austenite grain or twin boundaries. The apparent relationship between the sheaf arrangement of the product phase and the grains of the parent phase is not a usual feature of a reconstructive, diffusional transformation. The sheaf arrangement of the sub-units is illustrated in figure 2.3.

The macroscopic shapes of the α_b regions are found to differ from the austenite regions from which they formed, the shape change in the transformed region corresponding to an invariant-plane strain (IPS). The IPS has a significant shear component which could be expected to produce a substantial stored strain energy in the transformed region (Hehemann, 1970).

The invariant plane of the shape change corresponds to the habit plane of the ferrite plates; in this respect the transformation product shows a similarity to martensite (Christian & Edmonds, 1984). The origin of the IPS shape change is

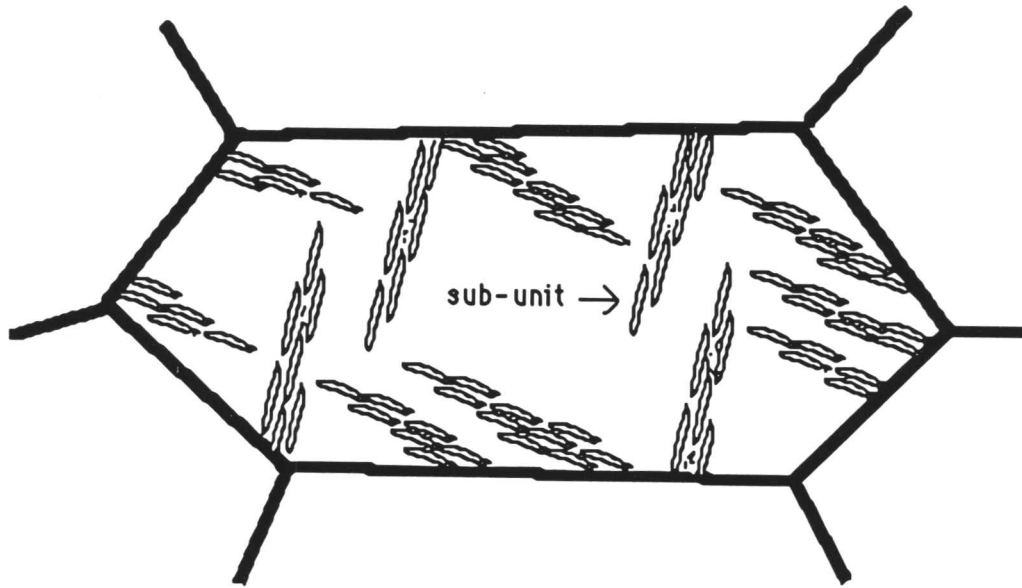


Figure 2.3: Arrangement of bainitic sub-units into sheaves within a prior-austenite grain

one of the major areas of dispute between contemporary hypotheses for a bainite reaction mechanism.

It has been suggested by Kinsman, Eichen and Aaronson (1975) that the observed IPS shape change arises during the growth of bainitic ferrite as a sessile α_b/γ semi-coherent interface is displaced by a step growth mechanism. They propose that a substantial barrier to growth of α_b develops at one orientation of the interphase boundary where ferrite and austenite lattices are sufficiently well-matched to form a partly-coherent misfit-dislocation interface. The matching is supposed to arise as a result of alignment of the close packed planes and directions in the two structures.

This boundary is then immobilized in a direction normal to itself and growth of the ferrite is then effected by the formation of ledges across the boundary.

The rate of growth of the bainitic ferrite under this mechanism is then governed by long term diffusion. In this way, it is claimed, the characteristic plate shape of ferrite develops, and the ledge migration produces ‘geometrical surface relief’ which is identified as a martensitic-type IPS on a macroscopic scale. As such, any similarity with the martensitic IPS would not necessarily demand an identical mechanism; the bainitic IPS would be consistent with a (carbon) diffusion-controlled growth process, along the lines of a bainite transformation mechanism of this type first proposed by Ko and Cottrell (1952).

It is similarly argued (Aaronson, Laird & Kinsman, 1970) that any surface relief effects associated with the IPS are not necessarily indicative of shear mechanism operation. Evidence in support of this supposition is cited from the formation of hexagonal close-packed γ -phase plates in the face-centred cubic α -phase in the Al-Ag system. In this case surface relief effects indicate an IPS (Liu & Aaronson, 1970), but Laird and Aaronson (1969) insist that the transformation mechanism involves diffusional jumps of silver atoms toward and aluminium atoms away from the edges of ledges formed on the faces of γ plates.

However, Bhadeshia and Edmonds (1979), argue that the IPS shape change necessarily implies an atomic correspondence between parent and product phase which is wholly inconsistent with a disordered diffusional transformation. It is suggested that the continuity of structure for such a coordinated movement of atoms requires a degree of atomic correspondence across all the interfaces of a product particle, and hence across a ledge structure. Thus the idea of a disordered ledge as proposed above is inconsistent with a coordinated movement of atoms.

It is concluded that the observed IPS arises due to a martensitic-type displacive transformation. The shape change will then give rise to a stored energy in the sheaves in the region of 400 Jmol^{-1} (Bhadeshia, 1981). The high dislocation density induced by attempts to relieve some of this strain energy by plastic deformation is then responsible for limiting the advance of the transformation interface and thus limiting the size of the bainitic sheaves (Bhadeshia & Edmonds, 1979). In this way, the observed limit on the growth of the bainitic regions in

the absence of any hard impingement or similar factor can be explained, as can the characteristic shape of the bainitic ferrite platelets.

Bhadeshia (1988) summarizes the bainite transformation as a displacive transformation with no diffusion of substitutional (or Fe) atoms across the transformation interface, referring to recent evidence from atom probe studies which demonstrates such an absence of diffusion across the transformation front (Stark, Smith & Bhadeshia, 1987).

2.2.2 Kinetic features of the transformation

In those alloy steels where a pronounced bay in the TTT curves is observed the bainite reaction (which corresponds to the lower C curve) can be studied carefully without interference from other, higher temperature transformations (Christian & Edmonds, 1984).

The bainite reaction exhibits all of the classical features of a nucleation and growth transformation except one: the reaction ceases before the carbon concentration in the retained austenite reaches that of the equilibrium or para-equilibrium phase boundary. The extent of reaction is a function of temperature, increasing as the transformation temperature is reduced. Extrapolation of this back to 0% bainite defines the kinetic bainite start temperature (B_s) above which bainite is not observed to form (Hehemann, 1970). The B_s is found to correspond approximately to the bay region in the TTT curve (Hehemann, 1970). These features of the bainite reaction (temperature dependence of fraction transformed, and existence of the B_s) are referred to as the *incomplete reaction phenomenon*.

Two contrary hypotheses have been advanced to explain the bay region in the TTT curve and the incomplete reaction phenomenon.

Kinsman and Aaronson (1967) postulate that the slowing down of reaction kinetics at the bay region arises due to a solute drag process caused by segregation of substitutional alloying elements across the austenite/ferrite transformation interface. It is propounded that the transformation is in reality continuous through the kinetic B_s , but that the effect of the solute drag process is to produce an apparent slowing in reaction kinetics at the bay, and the variant mor-

phologies observed above B_s (Hehemann, Kinsman & Aaronson, 1972); similar structures to bainite which form above the B_s temperature are cited as evidence for this proposal. This leads to the proposition that the observed transformation products are related by a continuum of transformation states. Purdy and Hillert (1984) extend this continuum through to lath martensite, which is seen as a kinetically-unstable extreme of the bainite reaction that is accompanied by effectively complete solute entrapment.

Contrary evidence from Bhadeshia and Waugh (1982) seems to suggest that segregation of substitutional alloying elements does not take place at the transformation interface. Significant supporting evidence for their results has been provided recently by further work on this problem involving a detailed atom probe study of the behaviour of substitutional atoms at the transformation interface (Stark, Smith & Bhadeshia, 1987). This leads to an alternative explanation for the features of the bainite reaction, which argues that a clear distinction between structures formed above B_s (*e.g.*, pro-eutectoid α_w) and bainite must be drawn. Different reaction mechanisms are operating (Christian & Edmonds, 1984), with products below B_s being produced by a transformation of a displacive character; it follows that the bay region can be explained as the point of overlap between two distinct C curves (for diffusional and displacive transformations), rather than a kinetic feature of a single transformation mechanism (Bhadeshia, 1988).

It has been noted that bainitic sheaves appear to originate at prior-austenite grain boundaries, and to be limited in their extent by hard impingement at those boundaries. As a consequence it is postulated that the austenite grain size, and hence the nature of the austenitizing treatment and in particular the temperature, can influence the kinetics of the transformation (Umemoto, Furuhashi & Tumura, 1986); in practice the effect of grain size on rate of transformation is found to be small (Umemoto, Horiuchi & Tumura, 1982).

2.2.3 Carbon content of bainitic ferrite

The carbon content of bainitic ferrite is of considerable significance in any attempt to develop a mechanism to explain the incomplete reaction phenomenon.

As an occupier of interstitial sites in the iron lattice, carbon has the ability to diffuse rapidly at temperatures low enough to reduce the rate of diffusion of substitutionals at the growth interface to negligible levels. It can be reasonably assumed that the reaction is brought to a halt by an increase in the carbon content of the retained austenite above some critical level. This must correspond to either a two phase equilibrium being achieved between ferrite and austenite, or a carbon enrichment of austenite to a point at which diffusionless growth is impossible (Bhadeshia & Edmonds, 1980).

Bhadeshia and Edmonds (1980) submitted that the carbon content is found in all cases to be considerably less than that expected for a diffusional growth process to be operating. They proposed that the undercooling in the bainite region is of a sufficient level as to give a $\gamma \rightarrow \alpha$ driving force high enough to cause α_b to be formed with a full supersaturation of carbon, which subsequently redistributes to the remaining austenite. Calculations predicting the time-scale of such redistribution at the order of only a few milliseconds (Kinsman & Aaronson, 1967), and thus entirely inconsistent with observed bainitic ferrite growth rates, have recently been corrected and modified (Bhadeshia, 1988); the resultant predicted redistribution times, of the order of a few seconds, are now in agreement with observed growth rates.

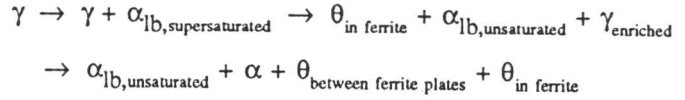
Thus, it may be suggested that bainite forms with supersaturation with respect to carbon by way of a martensitic-type nucleation process and growth of lath-like sub units. This is followed by a redistribution of carbon to the surrounding regions of remaining austenite, but after, rather than during, the formation of the bainite plate, as shown on figure 2.4 (Bhadeshia, 1981). Enrichment of the retained austenite progressively reduces the free energy driving force for bainite formation; the enriched austenite carbon concentration approaches the T'_0 curve, at which point the free energy available for transformation becomes insufficient to drive the displacive mechanism, no further bainite formation is possible, and the reaction then ceases. Thus, a model is provided by which it is possible to explain the incomplete reaction phenomenon, as is summarized in figure 2.5. It has been observed that carbon enrichment can dictate that

(a) Upper Bainite



(b) Lower Bainite

High dislocation density



Low dislocation density

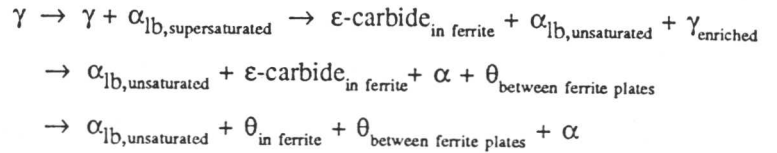


Figure 2.5: The bainite transformation (from Bhadeshia, 1988)

2.2.4.1 Upper bainite

This consists of aggregates of lath-, plate- or needle-like ferrite with carbides precipitated in the inter-lath regions. As the temperature is lowered, or the carbon content of the alloy increased, the laths become thinner and show an increased tendency to group together into sheaves, a process which has been entitled sympathetic nucleation (Aaronson, 1962), and the inter-lath carbides become near complete cementite films (Christian & Edmonds, 1984). The sub-units in such sheaves are observed to have the same habit plane with respect to the austenite from which they form, and a roughly parallel orientation in space (Ohmori, 1971). The width of these laths is observed to decrease as the transformation temperature is decreased, but the length remains fairly constant and is believed to be governed by prior-austenite grain size constraints (Pickering, 1967). Neither the sheaves, nor their constituent sub-units, are found to extend across prior-austenite grain boundaries, which is consistent with a displacive mechanism for their formation.

On the basis of several observed rational orientation relationships between

the inter-lath carbides and the original austenite it is assumed that these carbides are formed directly from the austenite rather than from the bainitic ferrite; hence, interlath carbide precipitation may be absent in some steels containing alloying elements that suppress cementite formation by raising the activity of carbon within austenite (especially silicon), which will generally result in carbon-rich austenite films being retained between the bainite laths after transformation.

2.2.4.2 Lower bainite

The lower temperature morphology is similar to upper bainite, but cementite or ϵ -carbide is found also within the α_b laths; these microstructural differences provide the foundation for the definition of the two categories of bainitic morphology, first suggested by Mehl (1939). In most steels the transition to lower bainite occurs at around 350°C (a temperature which shows little composition dependence according to Christian and Edmonds (1984)), although higher temperatures have been noted for some steels (*e.g.*, Pickering (1967) recorded a transition as high as ~550°C for 0.5 wt% Mo steels at around 0.5 wt% C). There is usually a short transition range over which both morphologies are exhibited.

It is suggested that the different morphologies are attributable to differing mechanisms by which decarburization of the supersaturated bainitic ferrite proceeds. The decarburization process is controlled by the diffusivity of carbon. At higher temperatures the carbon is able to diffuse sufficiently quickly to be expelled into the interlath austenite. As the temperature reduces, the carbon diffusion rate becomes insufficient to allow complete unsaturation of the bainitic ferrite by carbon diffusion into austenite; hence decarburization of bainite is then effected, at least in part, by cementite precipitation. It is found that very-low-carbon steel will not form lower bainite, since the free energy driving force for cementite precipitation will never be high enough to make it preferable to carbon diffusion into retained austenite as a mechanism of decarburization of supersaturated ferrite.

The intra-bainitic carbides are typically orientated at about 60° to the long axis of the α_b laths. Bhadeshia (1980) has asserted that the absence of a reproducible orientation relationship between austenite and intrabainitic cementite

indicates that these carbides are generated from supersaturated bainitic ferrite, rather than at the growth interface between α_b/γ during growth of the bainite sheaves as had previously been suggested by some authorities. The nature of the carbides within the ferrite is then determined by the dislocation density generated in the bainite before precipitation of carbides takes place: at high dislocation density, carbon associated with the dislocations allows direct precipitation of cementite at these sites, so that ϵ -carbide formation is disfavoured. According to this hypothesis ϵ -carbide should not be present in steels of C < 0.55 wt% (Bhadeshia, 1980), which is in good agreement with practical observations.

2.2.5 Conclusions

The considerable controversy attached to various aspects of this transformation as set out above are unlikely to be wholly resolved for some time. Whilst it is impossible fully to discount a carbon-diffusion-controlled growth mechanism for bainite, the balance of recent evidence is in favour of Hehemann's mechanism of nucleation and martensitic-type growth of lath-like sub-units. Thus, bainite forms through a displacive transformation, and as such by way of a mechanism distinct from that which generates pro-eutectoid ferrite and pearlite, and the bay in TTT curves for alloy steels is attributable to this (the curves are, in fact, separate curves representing diffusional and displacive products) rather than to a solute drag process at the transformation interface.

2.3 Carbide Precipitation in Allotriomorphic Ferrite

It is a fundamental feature of the iron-carbon system that carbon solubility is much greater in austenite than it is in ferrite under the same conditions; thus, precipitation of carbides during the austenite–ferrite transformation is likely to play a significant part in the transformation for all but the lowest carbon steels. In plain carbon steels carbide precipitation is in the form of discrete cementite particles or pearlitic nodules after substantial ferrite growth. Addition of alloying elements can lead to precipitation of alloy carbides instead of iron carbides, and such carbide structures play a significant rôle in contributing to the creep strength of low-alloy ferritic creep resistant steels. In addition, if

the alloying elements are strong carbide formers, then ferrite growth may be restricted by the need for alloying elements to partition by diffusion, and the carbide may then be observed to grow simultaneously with ferrite (Honeycombe & Pickering, 1972). The most important forms of alloy carbide precipitate found in steels are summarized below, categorized according to precipitation site.

2.3.1 Interphase precipitation

This is the term given to arrays of fine, evenly spaced precipitates, which have been noted as being desirable to enhance creep properties. Interphase carbide precipitates frequently occur in banded structures within the ferrite grain, but irregular dispersions are also observed. These precipitates are believed to form during the transformation to ferrite, being nucleated at the α/γ interface as the ferrite region grows (Davenport, Berry & Honeycombe, 1968). The process is of particular importance in microalloyed steels containing niobium, vanadium and titanium, but in higher alloy steels coarser precipitates related to Fe_3C are also observed (Honeycombe, 1984). Honeycombe classifies interphase precipitation into two forms, depending on the nature of the interface between the growing ferrite and retained austenite.

2.3.1.1 Planar interphase precipitation

Planar arrays of precipitates are found to be associated with low-energy, semi-coherent, planar (faceted) α/γ growth interfaces. Edmonds and Honeycombe (1978) found that such boundary structures are very common at all transformation temperatures on a local scale, and planar interphase precipitation is not confined to those transformation products (*e.g.*, Widmanstätten ferrite) where the presence of such boundaries on a larger scale is well known; indeed interphase precipitation is much more common in fully equiaxed ferrite than in Widmanstätten ferrite.

These semi-coherent interfaces are associated with step migration during ferrite development (see figure 2.6). Regularly-spaced steps give rise to evenly-spaced precipitate arrays (marked a on figure 2.6) and irregular steps produce irregularly-spaced arrays (b). Note that precipitation does not usually occur at

the high-energy, high-angle interfaces at the transformation front (*i.e.*, the step faces); growth rates are too high to allow sufficient diffusion to the precipitate site. On the occasions when there is precipitation the step movement is impeded or stopped, leading to a discontinuity in the array. Instead, precipitation takes place on the low-energy, less mobile interfaces. There is typically an orientation relationship across the transformation interface of the Kurdjumov-Sachs (K-S) form (Honeycombe, 1984), viz:

$$\langle 111 \rangle_{\gamma} \parallel \langle 110 \rangle_{\alpha} \quad \{ \bar{1}\bar{1}0 \}_{\gamma} \parallel \{ \bar{1}\bar{1}1 \}_{\alpha}$$

The interphase plane for such precipitation is normally $(111)_{\gamma} \parallel (110)_{\alpha}$ and this will be reflected in the crystallography of the precipitates (Honeycombe, 1984).

Precipitates found in association with planar austenite/ferrite interfaces include VC, NbC, TiC, TaC, Cr₂₃C₆, Cr₇C₃, M₆C, W₂C, Mo₂C, ϵ -Cu and Au (the last two are not carbide structures but are observed to precipitate and behave in the same way). The crystallography of these precipitates is listed in table 2.1 (from Honeycombe, 1984).

Phase	Structure	Habit	Orientation relationship with α matrix
VC, NbC, TiC, TaC	fcc	plates	$(100)_p \parallel (100)_{\alpha} : [010]_p \parallel [110]_{\alpha}$ (Baker-Nutting)
Cr ₂₃ C ₆	complex cubic	rods or laths	$(111)_{\text{Cr}_{23}\text{C}_6} \parallel (101)_{\alpha} : [\bar{1}10]_{\text{Cr}_{23}\text{C}_6} \parallel [\bar{1}11]_{\alpha}$ (Kurdjumov-Sachs)
Mo ₂ C	c-p hex.	rods, $[100]_{\alpha}$ growth dir.	$(0001)_{\text{Mo}_2\text{C}} \parallel (011)_{\alpha} : [2\bar{1}\bar{1}0]_{\text{Mo}_2\text{C}} \parallel [100]_{\alpha}$
ϵ -Cu, Au	fcc	spheres, rods	$(111)_{\epsilon\text{-Cu}} \parallel (101)_{\alpha} : [\bar{1}10]_{\epsilon\text{-Cu}} \parallel [\bar{1}11]_{\alpha}$ (Kurdjumov-Sachs)

Table 2.1: Crystal structures of common interphase precipitates in ferrite (Honeycombe, 1984)

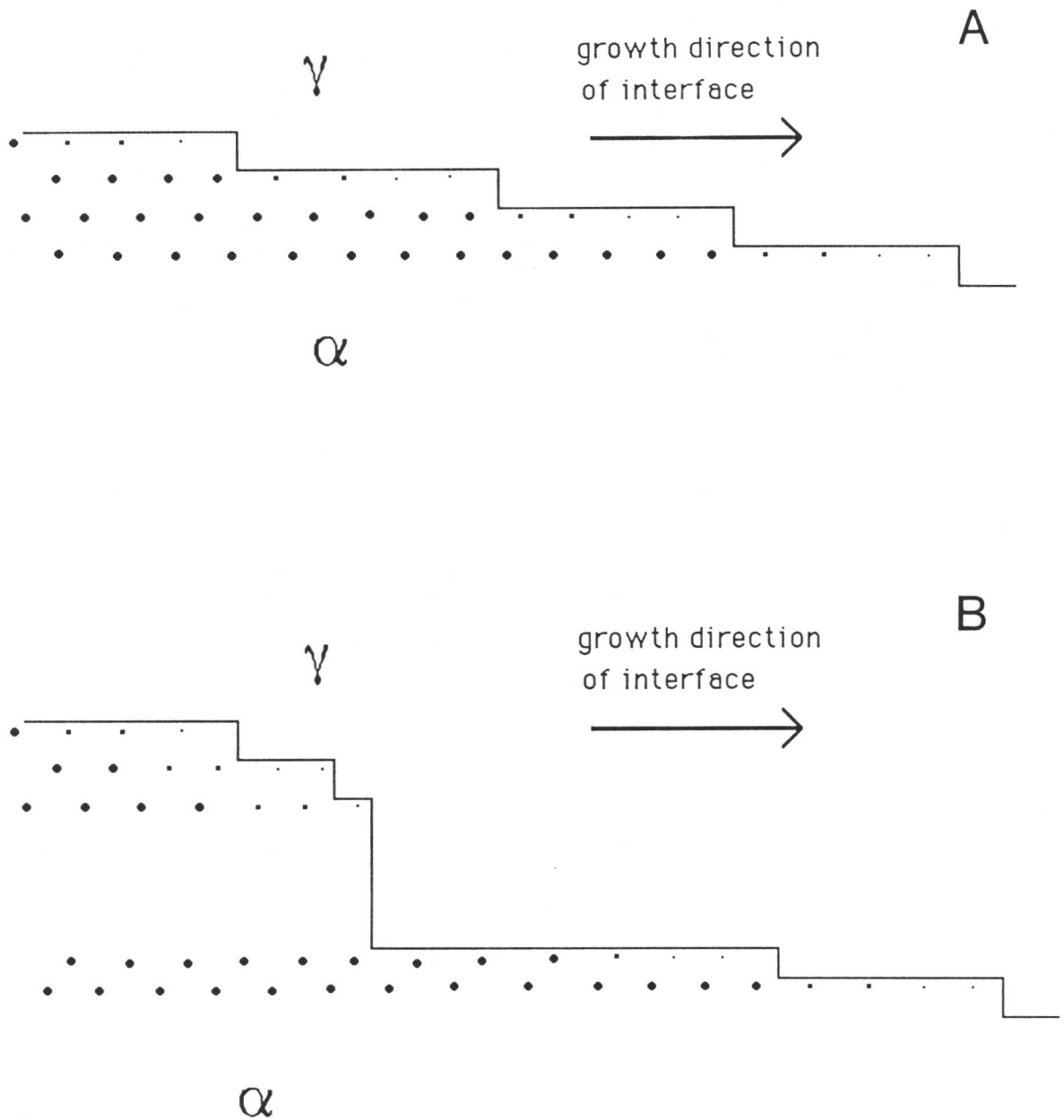


Figure 2.6: Planar interphase precipitation (from Honeycombe, 1984)

2.3.1.2 Non-planar interphase precipitation

In these cases the precipitates are believed to be associated with high-energy, incoherent α/γ interfaces, forming into irregularly organized periodic arrays. Campbell and Honeycombe (1974) conjecture that the arrangement of such particles is determined by the pinning action of the precipitate on the α/γ growth front. As a result of such pinning, the interface is forced to bow around in a way analogous to Orowan bowing of dislocations if the transformation is to advance, which gives rise to an irregularly orientated array of still regularly-spaced

precipitates.

Non-planar precipitate arrays are especially prevalent for coarser Cr_7C_3 and Cr_{23}C_6 types, and for other alloy systems where the precipitates are generally coarser and more widely spaced (Honeycombe, 1984).

2.3.2 Fibrous carbide precipitation

Fibrous carbide structures are found to precipitate in many of the steels that exhibit interphase precipitation, often under the same conditions and at the same time; for example, Mo_2C , VC, TiC, NbC, Cr_{23}C_6 , Cr_7C_3 , $\epsilon\text{-Cu}$ and Au are all observed in this morphology. The fibrous structures are typically 100–300Å in diameter, 200–500Å apart, and with a length of the order of several μm (Honeycombe, 1984). In some cases, *e.g.*, with chromium steels transformed at higher temperatures, the structures have been found to be directly analogous to cementite (Campbell & Honeycombe, 1974), but as a general rule important differences are found in the alloy carbide morphologies, such as an almost total absence of branching.

As was the case for interphase precipitation, fibrous carbides are found to be associated with the austenite/ferrite interface, nucleating at incoherent boundaries, and growing in a direction approximately normal to the transformation front (Davenport, Berry & Honeycombe, 1968); both forms of precipitation have been noted in the same steel in many cases. The exact nature of the α/γ interface is thus very important in determining the relative proportions of fibrous and interphase precipitation in cases where both are found to occur, and this is in turn dependent on the transformation conditions. Investigations have shown that fibrous precipitation predominates for longer reaction times, whether this arises as a result of alloying (Batte & Honeycombe, 1973), or reduction of the temperature (Berry & Honeycombe, 1970).

2.3.3 Precipitation on dislocations

At higher undercoolings the ferrite can, to some extent, remain supersaturated throughout the transformation such that the precipitation processes documented above, associated with the austenite/ferrite transformation front, do not take

place. Subsequent precipitation can then occur on sites such as dislocations within the ferrite and at α/α grain boundaries, which provide lower energy locations for heterogeneous nucleation of intragranular precipitates. Dislocations are generated in the transformed region as a result of the volume change from γ to α ; higher dislocation densities are found in Widmanstätten ferrite than in equiaxed ferrite, probably reflecting shear processes in α_w formation (Smith & Honeycombe, 1982). Such precipitation has been noted by Ballinger and Honeycombe (1980) for VC in low-carbon vanadium steels, and by Ricks, Howell and Honeycombe (1980) for ϵ -copper in Fe–Cu–Ni alloys.

2.3.4 Precipitation at austenite grain boundaries

Precipitation has been found to take place in some cases at the prior austenite grain boundaries, even preceding the initiation of ferrite formation (Honeycombe, 1984). Grain-boundary precipitation is also observed at heterogeneous sites on newly-formed ferrite grain boundaries during transformation. Carbides generated in this way are generally found to be much coarser than interphase precipitates, and as such regarded detrimental to creep strength in creep resisting steels of the class under investigation in this project; grain boundary precipitation is therefore to be avoided in low-alloy ferritic creep resisting steels.

2.3.5 Summary

In general, creep resisting properties are optimized by the generation of a fine dispersion of regularly-spaced alloy carbide particles, rather than coarser or fibrous structures (Cane & Townsend, 1984). A consideration of the above alloy carbide precipitation routes is therefore of substantive importance in determining heat treatments to maximize creep life. The carbide structures actually produced in creep resistant boiler system steels are considered, along with their behaviour under service conditions, in a later section.

2.4 Changes in Alloy Carbides Within the Ferrite During Ageing

The microstructure of the low-alloy ferritic steel found in power station headers is relatively fine-grained. The material can be considered to achieve creep re-

sistance from particle dispersion, and to accumulate damage by degradation of the precipitate structure, which can occur in two ways.

- (i) Particle coarsening due to diffusion at the elevated service temperature (with a concomitant increase in particle spacing), leading to a particle dispersion which is no longer optimal for creep properties.
- (ii) Ageing during service where the carbide in the initial structure is not the equilibrium phase at the ageing temperature may result in precipitation of other (more stable) carbides with properties detrimental to creep behaviour. This will frequently be compounded by loss of the beneficial carbide structures as they go back into solution.

It has been postulated by several workers that monitoring of carbide structure may supply the means to assess creep damage accumulation levels in those materials where degradation of the precipitate structure is the dominant damage mode. In addition, such work could provide a basis for mechanistic creep damage models to be developed for the creep processes in these materials.

Some of the earliest quantitative analysis of carbide compositions during creep was performed by Murphy and Branch (1969). Working with turbine casing steels of both 1Cr–Mo–V and $2\frac{1}{4}$ Cr–Mo–V type,¹ they observed that during ageing at 575°C there was a tendency for coarse M_3C carbides to form. These will denude the surrounding region of chromium, molybdenum and vanadium, and hence reduce the quantity of the fine alloy carbides (in these cases they were observed to be primarily vanadium carbides) that provide the creep strength, which will therefore be reduced during ageing. The effect of dissimilarities in composition between different casts (see the footnote) on creep properties was also highlighted; although in this case molybdenum and chromium carbides were

¹ a number of different steels of either general class were used, with actual compositions (in wt %) within the following ranges:

1Cr type: 0.11–0.13C, 0.49–0.58Mn, 0.68–0.98Cr, 0.09–0.28Ni, 0.77–1.06Mo, 0.14–0.24Cu 0.23–0.32V, 0.27–0.47Si wt%;

0.25Cr type: 0.11–0.17C, 0.51–0.60Mn, 0.28–0.32Cr, 0.05Ni, 0.48–0.50Mo, 0.05Cu, 0.25–0.26V, 0.25–0.27Si wt%.

not believed to be directly critical for creep strength, Murphy and Branch noted that the amount of coarse M_3C formed was closely related to chromium and molybdenum concentrations. As a result the contribution of M_3C to the creep strength was similarly related to concentrations of the alloying elements other than vanadium. It was concluded that segregation effects involving alloying elements that do not form the precipitate dispersion which gives the creep strength can also, indirectly, have a significant local effect on that creep strength.

A study by Collins (1978) on $\frac{1}{2}Cr-\frac{1}{2}Mo-\frac{1}{4}V$ (approximate compositions) steam pipe material removed from service revealed Mo_2C as the predominant carbide within the ferrite. However, when accelerated creep testing was performed by raising the temperature, VC was observed to be more abundant. Closer examination showed that the carbides were in the form of a capital-H-shaped structure, with Mo_2C forming the uprights and VC the crossbar. The Mo_2C appeared to go back into solution if the material was heated to $690^\circ C$ after exposure at the service temperature leaving only narrow rods of VC. Collins questions the wisdom of accelerated creep testing by raising the temperature in such materials, where the carbide structure changes fundamentally between service and test temperatures.

The 'H' carbide structures have been found to be associated with dislocations, although VC precipitation is also observed at points within the bulk material where high dislocation densities are not found (Williams, 1981). Williams suggested that VC was precipitated as a metastable carbide form during fabrication, but that Mo was able to diffuse along the easy diffusion paths provided by dislocation pile ups associated with some of the VC precipitates. This provided a mechanism by which Mo_2C , the more stable form at service temperatures and below, could form at these points. Ultimately during service VC is replaced entirely by the more stable carbide form, which is also coarser, less evenly distributed, and hence detrimental to creep properties. Note that this is completely the reverse of what happens during accelerated creep testing above $690^\circ C$ (Collins, 1978, above) where Mo_2C appears the less stable form and is replaced by VC in time; great doubt must be cast on the representativity of

accelerated temperature testing in these materials.

For non vanadium containing steels of the $2\frac{1}{4}\text{Cr}-1\text{Mo}$ class Williams (1981) found Mo_2C to be the precipitate of most relevance to creep strength. This was observed to coarsen during service, in particular where associated with dislocations. As a result the precipitate structure became much more irregular, as well as coarser, to the detriment of the creep strength.

More detailed work on changes in carbide composition in a $\frac{1}{2}\text{Cr}-\frac{1}{2}\text{Mo}-\frac{1}{4}\text{V}$ type steel² (Carruthers & Collins, 1983) confirmed VC as the primary carbide, but initially containing up to 30 wt% molybdenum (typical levels were around 10 wt%) with a little chromium, manganese and iron in place of some of the vanadium. After exposure at 575°C, the proportion of molybdenum in the alloy carbides had increased; compositions in the range 5–100 wt% vanadium and 0–85 wt% molybdenum were recorded. It is submitted that the variations illustrate local differences in ease of diffusion of Mo to the VC, the process that effects the replacement of V by Mo to form the more stable carbide structure.

Carruthers and Collins also noted the substitution, to some extent, of chromium for iron in Fe_3C , a process which was found to show a significant temperature dependence (chromium content in the cementite had risen to 10 wt% in 125 hours at 625°C but 8000 hours at 575°C was needed for a similar effect). It has been suggested that there is a potential use for chromium concentration in cementite as a method of determining a representative thermal history of the component

To summarize the above we can say the following.

- (i) MC carbides in Cr–Mo–V class steels are replaced by M_2C over a period of exposure at temperatures lower than 600°C.
- (ii) At a greater temperature MC remains the more thermodynamically stable form and is not replaced. Hence experimental results obtained in this temperature regime cannot be reliably extrapolated to service conditions, and

² actual compositions (in wt %) were in the ranges: 0.11–0.13C, 0.26–0.28Si, 0.42–0.52Mn, 0.010–0.011P, 0.55–0.56Mo, 0.35–0.36Cr, 0.03–0.17Ni, 0.12–0.19Ni, 0.010–0.011Sn, 0.25–0.32V.

results obtained which rely on such an extrapolation must be treated with great caution.

- (iii) In Cr–Mo type steels M_2C is the more thermodynamically stable form at both the service and at elevated temperatures so extrapolation of results from higher temperatures to the service temperature is not invalidated in the same way as for the Cr–Mo–V steels.
- (iv) Particle size measurements do not appear to provide an accurate or reliable method of remanent life determination.
- (v) Chemical analysis of both the primary alloy carbides and the cementite may enable improved determination of remanent life, even in the absence of a direct mechanistic relationship to creep damage, by providing a representation of the effective temperatures experienced during service by a particular component (Carruthers & Collins, 1983, for example).

2.5 Cavitation During Creep

It was noted that for low-alloy ferritic steels creep damage accumulation occurs via microstructural degradation (particle coarsening leading to a loss of the optimum precipitate distribution) or void accumulation. For the sake of completion the latter process is considered briefly in this section.

In general, cavitation is the predominant damage mode in low-alloy ferritic steels where the microstructure is coarser grained. A greater susceptibility to this mode of damage accumulation is also exhibited in higher alloy steels and at higher creep strain rates (Dyson, 1976). Thus, in the majority of situations relating to low-alloy ferritic steel steam header bulk material, cavitation can be expected to be of reduced significance (but in isolated positions local variations in material properties and conditions could increase the tendency for cavitation). Formation of cavities is of most relevance in relation to creep damage accumulation in the coarser grained heat affected zone region of welds and weldments within the power station boiler system (Cane & Townsend, 1984).

2.5.1 Initiation of cavities

Cavities may nucleate homogeneously either at the grain boundaries or in the bulk grain due to shear deformation caused by the applied stress. However, it has been proposed (Cane, 1976) that typical low-alloy ferritic steels, where cavitation is the predominant damage mode, will nucleate cavities in a heterogeneous manner on non-wetting grain boundary precipitates. Dislocation pile up at the precipitate caused by localized deformation makes such a precipitate a highly-favoured cavity nucleation site.

Cane (1979), performed work on $2\frac{1}{4}\text{Cr}-1\text{Mo}$ steel³ with a coarse bainitic microstructure achieved by austenitizing at 1300°C for 1 hour and air cooling, followed by 4 hours at 700°C . Cane observed the cavities and found them to be distributed heterogeneously throughout the prior-austenite grain boundaries. They were associated in particular with M_{23}C_6 particles, and found to nucleate in the very early stages of exposure. The quantities present showed relatively little sensitivity to effective mean stress levels for a given strain, but instead appeared to be dependent on the magnitude of the maximum principal stress.

Similar observations of heterogeneous cavity nucleation at grain boundary precipitates (especially alloy carbides) during secondary creep have been made for other steels (*e.g.*, Needham & Gladman, 1980; Dyson, 1976).

2.5.2 Cavity accumulation and growth

Various models have been proposed for the growth of cavities during ageing of these materials. The majority of early analyses used as a basis the diffusional growth concept proposed by Balluffi and Seigle (1957), which involves diffusion of atoms from the cavity surface to other parts of the grain boundary region more favourably orientated to the maximum principal stress. More recent work has exposed limitations in such a model.

Dyson (1976) conjectured that in some circumstances growth by a diffusion mechanism would be constrained by the creep deformation process in polycrystals. He suggested that vacancy diffusion could provide only an upper bound

³ specifically, Fe-2.25Cr-1.0Mo-0.48Mn-0.48Si-0.18Ni-0.06As-0.02P-0.02S-0.02Sn-0.11C wt%.

growth rate, with the lower bound being determined by the mean applied shear stress rather than the maximum principal stress. Any constraint is likely to be most marked in higher alloy materials (with high cavitation densities of non-uniform distribution) and at higher strain rates, so is of limited significance in the case of low-alloy ferritic steel steam headers.

In Cane's study (1979, see above) the growth rate was monitored for various maximum principal stresses (σ_1) at constant mean effective stress ($\bar{\sigma}$), and for various σ_1 at constant $\bar{\sigma}$. Cavities were found to grow initially in a spherical manner, but as they became larger ($> 1\mu\text{m}$) growth proceeded by spreading across the grain boundary area and by accumulation of several voids into one larger cavity.

The growth rate appeared to depend more on $\bar{\sigma}$ than σ_1 when circular notch tests were carried out. At low ($< 150\text{ MPa}$) stress the growth rate appeared to be proportional to the creep rate in a uniaxial system. Cane therefore suggests that the diffusional growth model requires considerable modification in order to take account of the tendency for voids to grow along the favourable grain boundary regions, and to cope with the real engineering situation of complex, multiaxial stress systems.

2.6 Ageing Behaviour of Bainitic Cementite

2.6.1 Composition change as an indicator of thermal history

Carruthers and Collins (1983) commented on the possibility of using changes in composition of cementite during service as a route to a more accurate determination of the thermal history of the component in question. Creep resistant steels typically contain bainitic regions (see above, where the typical mixed allotriomorphic ferrite/bainite microstructures in low-alloy ferritic creep resistant steels was discussed). Cementite is also found in a pearlitic region in some of these materials.

Even in those creep resistant steels where pearlitic cementite is observed, it does not seem feasible to extrapolate thermal history from cementite composition for a number of reasons, namely: initial composition lies between

equilibrium and paraequilibrium (figure 2.7), and no sound theory exists to calculate the starting composition exactly; pearlitic cementite composition is frequently found to vary as a function of distance from the austenite/ferrite interface (Chance & Ridley, 1981, *et al.*); and the mean starting composition may show a size dependence. Without a knowledge of the starting composition, no fundamental model could be constructed to chart the approach of the cementite composition to equilibrium during ageing.

Bhadeshia proposes that the lower transformation temperature and higher driving force for cementite formation from carbon-enriched austenite during the bainite transformation, and the consequent negligible redistribution of substitutional alloying elements during the transformation, means that such difficulties as are encountered in pearlite are considerably reduced; therefore, the use of carbide compositional changes to determine thermal histories is a practical option. Although similar problems are encountered for both pearlite and bainitic cementite, in that no rigorous model for predicting θ composition immediately after the transformation exists, the composition change in bainitic cementite during ageing could still be modelled provided the original redistribution of substitutional alloying elements during transformation was sufficiently small to be negligible relative to the composition changes owing to diffusion (as the cementite moves towards an equilibrium composition of substitutionals) occurring over longer time scales.

Experimental evidence that this condition holds for the bainite reaction is provided by Hultgren (1947), who observed that bainitic cementite had a substitutional alloy content only just above that of the material as a whole, and very much less than would be expected for pearlite where appreciable redistribution of substitutional alloying elements does take place. More recent work by Chance and Ridley (1981) confirmed that k_{Cr} (the partition coefficient, wt % Cr in θ / wt % Cr in α_b) was very close to unity (figure 2.7). All the experimental data indicate that there is very much less partitioning during the growth of bainitic cementite than there is during the growth of pearlitic cementite.

During tempering in service the equilibrium composition can be expected

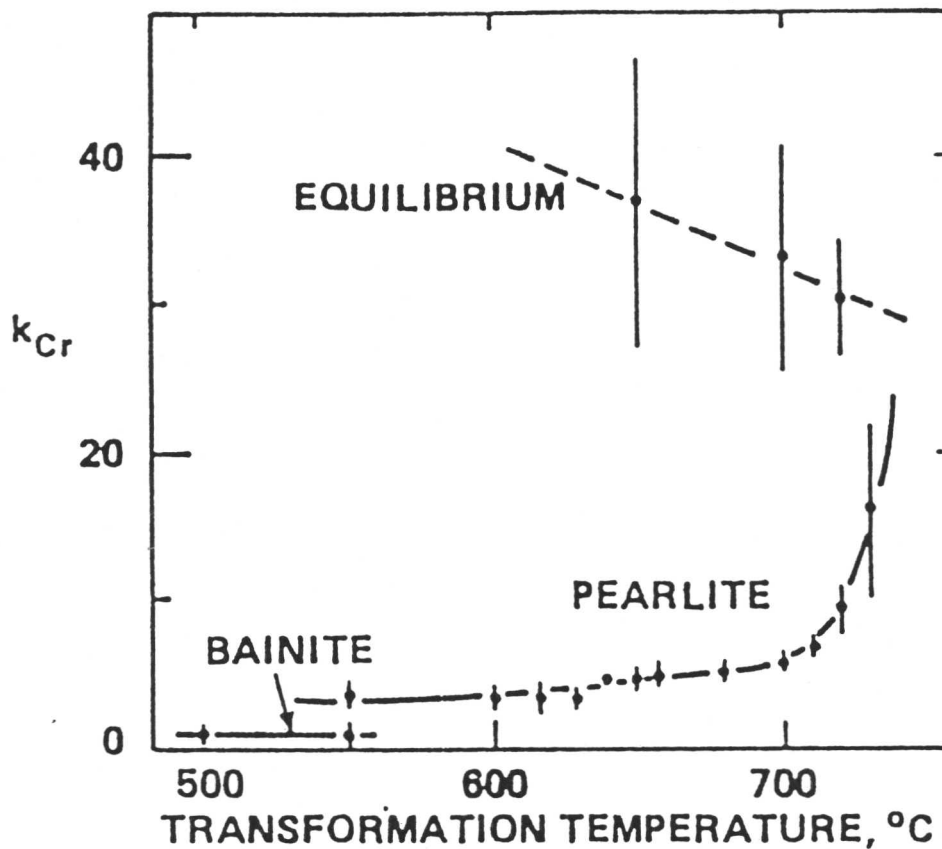
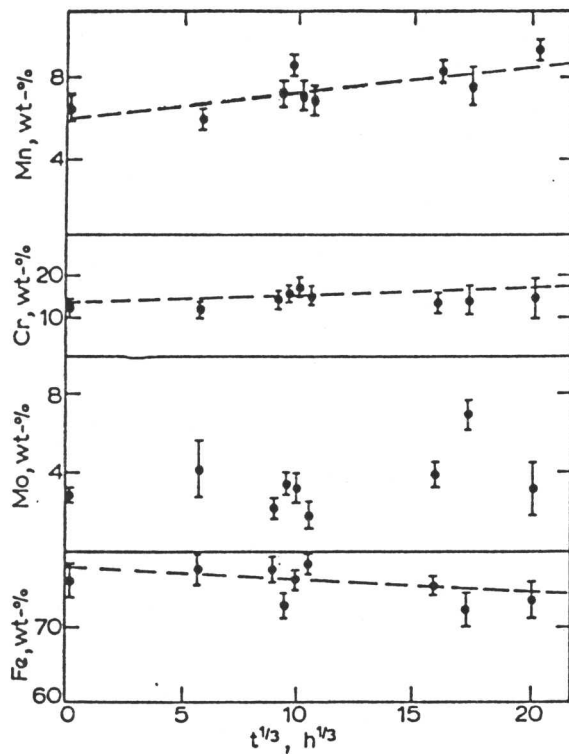


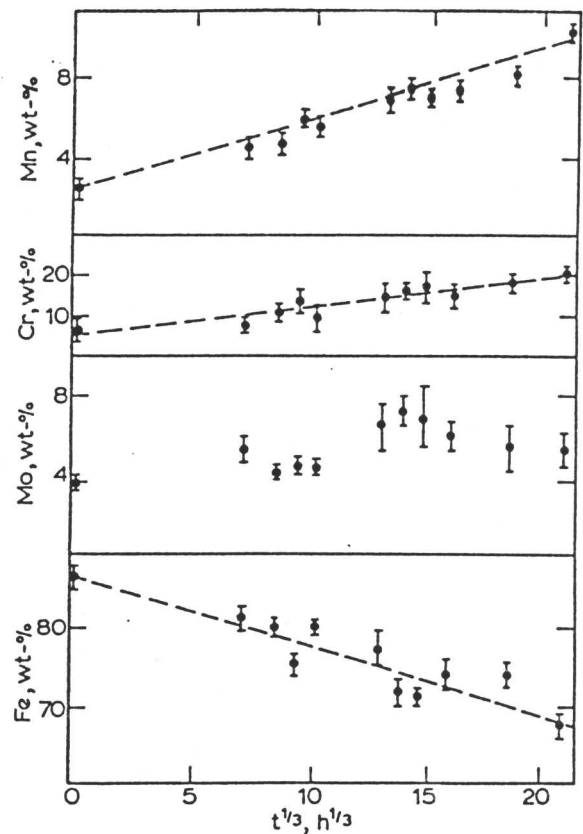
Figure 2.7: Variation of cementite composition with transformation temperature following isothermal transformation (Chance & Ridley, 1981)

to be approached in a manner dependent on initial composition, microstructure and conditions. This approach was applied by Carruthers and Collins (1981) to determine a relationship between cementite composition and ageing time. They found that the chromium and manganese concentrations in pearlitic cementite increased according to an approximately $(\text{time})^{1/3}$ relationship, a relation which tries to model enrichment based upon particle coarsening theory, rather than on diffusion of substitutionals within the ferrite; this condition has not been justified theoretically.

Composition change measurements which appear to be in accordance with a relationship of the $(\text{time})^{1/3}$ type have subsequently been observed for bainitic



partially service exposed



regenerated material

Figure 2.8: Change in substitutional alloying element concentrations in cementite during ageing (Afrouz, Collins & Pilkington, 1983)

cementite using service exposed 1Cr- $\frac{1}{2}$ Mo material⁴ (for 70000 hrs at 565°C) (Afrouz, Collins & Pilkington, 1983). Chromium and manganese concentrations in bainitic M_3C were found to increase in a similar manner to that noted for pearlite, an approximately $t^{1/3}$ relationship (figure 2.8).

It is apparent that the time^{1/3} relationship cannot continue indefinitely, and the composition versus time^{1/3} graph will flatten out as the limiting situation of equilibrium composition is approached. The equilibrium concentrations (in wt %) in ferrite and cementite have been calculated for both the service and the test temperatures for the material used by Afrouz, Collins and Pilkington

⁴ specifically, Fe-0.84Cr-0.48Mo-0.48Mn-0.24Si-0.07Ni-0.04P-0.035S-0.02V-0.11C wt %

(Bhadeshia, 1989), and were found to be:⁵

Element	$\alpha(976\text{K})$	$\theta(976\text{K})$	$\alpha(823\text{K})$	$\theta(823\text{K})$
Cr	0.52	21.3	0.30	36.0
Mo	0.40	5.8	0.34	9.3
Mn	0.38	6.7	0.29	13.2

To summarize, determination of a rigorous model based on the diffusion processes involved during the ageing of these materials could enable cementite compositions to be monitored in order to provide information on thermal history in the manner suggested by Carruthers and Collins, thence generating improved remanent life estimates. A condition of such a procedure, however, is that the time taken for equilibrium concentrations to be approached must be of the same order as component life time (*i.e.*, the composition must be changing throughout the service life of the material).

2.6.2 A theoretical analysis of the composition change

As was noted above, the classical approach has been to relate composition change with the coarsening of cementite during ageing, leading to a predicted variation of composition with time^{1/3}. This relationship has met with limited experimental success in some cases. Nevertheless, it is imperative that an approach based on a consideration of the enrichment of cementite by way of diffusion of substitutional alloying element atoms within the bainitic ferrite be used, if a model of real physical significance is to be developed.

A simple analytical approach, which is limited to the case where no soft impingement occurs in the ferrite, can be obtained by considering a cementite slab in an infinite ferrite matrix (Bhadeshia, 1988). The cementite slab is assumed to have a composition, c^θ , which does not vary with distance from the interface, and the composition of the ferrite, c^α , is assumed to be $c^{\alpha\theta}$ at the

⁵ Note that these are specific to this particular alloy (although it has a composition sufficiently close to that of the material used in this programme that these figures can be taken as an approximate guide to that material also.)

interface and \bar{c} at infinity. If the cementite portion has a thickness x_θ , and t_c is taken to be the time required for that slab to reach a concentration c^θ , then a standard mass balance procedure requires that:

$$0.5x_\theta(c^\theta - \bar{c}) = \int_0^\infty \bar{c} - c^\alpha(x, t_c) dx \quad (2.1)$$

where

$$c^\alpha(x, t_c) = \bar{c} - (\bar{c} - c^{\alpha\theta}) \operatorname{erfc} \left\{ \frac{x}{2\sqrt{D_\alpha t_c}} \right\} \quad (2.2)$$

hence

$$0.5x_\theta(c^\theta - \bar{c}) = (\bar{c} - c^{\alpha\theta}) \int_0^\infty 1 - \operatorname{erf} \left\{ \frac{x}{2\sqrt{D_\alpha t_c}} \right\} dx \quad (2.3)$$

where t_c is the time to reach cementite of concentration c^θ ,

\bar{c} is the mean alloy composition,

x_θ is the cementite particle size,

$c^{\alpha\theta}$ is the composition of α in equilibrium with θ ,

and D_α is the diffusivity in ferrite.

A substitute variable, y , is defined such that

$$y = \frac{x}{2\sqrt{D_\alpha t_c}} \quad dy = \frac{dx}{2\sqrt{D_\alpha t_c}} \quad (2.4)$$

and substituting y in equation (2.3), and redefining the upper limit of the integral in equation (2.3) to be a finite variable, y' , yields equation (2.5)

$$0.5x_\theta(c^\theta - \bar{c}) = 2\sqrt{D_\alpha t_c}(\bar{c} - c^{\alpha\theta}) \int_0^{y'} 1 - \operatorname{erf}\{y\} dy \quad (2.5)$$

But

$$\int_0^{y'} \operatorname{erf}\{y\} dy = \left[y \operatorname{erf}\{y\} - \frac{(1 - e^{-y^2})}{\sqrt{\pi}} \right]_0^{y'} \quad (2.6)$$

hence equation (2.5) becomes

$$0.5x_{\theta}(c^{\theta} - \bar{c}) = 2\sqrt{D_{\alpha}t_c}(\bar{c} - c^{\alpha\theta}) \left[y - y\text{erf}\{y\} + \frac{(1 - e^{-y^2})}{\sqrt{\pi}} \right]_0^{y'} \quad (2.7)$$

Let $y' \rightarrow \infty$; then $\text{erf}\{y'\} \rightarrow 1$, $e^{-y'^2} \rightarrow 0$, and $y' - y'\text{erf}\{y'\} \rightarrow 0$; and equation (2.7) can be simplified to

$$0.5x_{\theta}(c^{\theta} - \bar{c}) = \frac{2\sqrt{D_{\alpha}t_c}(\bar{c} - c^{\alpha\theta})}{\sqrt{\pi}} \quad (2.8)$$

It follows that

$$t_c = \frac{\pi[x_{\theta}(c^{\theta} - \bar{c})]^2}{16D_{\alpha}(\bar{c} - c^{\alpha\theta})^2} \quad (2.9)$$

This gives a working relationship between ageing time and composition for plate-like cementite particles which will remain valid until the onset of soft impingement in ferrite (typically about 8000 hours of service life in power plant materials); that is, the equation will be applicable to the early stages of the ageing process in these materials, especially in respect of the properties of the equation noted below.

- (i) The time taken for the cementite to reach a given concentration varies with the square of particle thickness; or conversely, composition varies with the reciprocal of the square of the particle thickness for different particles aged over a given time.
- (ii) The composition of cementite of a given x_{θ} should vary with $(\text{time})^{1/2}$ rather than the $(\text{time})^{1/3}$ relationship proposed by Afrouz *et al.* (1983). It is noted that the data used by Afrouz *et al.* in fact fits the $(\text{time})^{1/2}$ relationship as well as (if not better than) the $(\text{time})^{1/3}$ relationship (see figure 2.9).
- (iii) The temperature dependence of the process can be attributed mostly to D_{α} , given that $c^{\alpha\theta}$ is a relatively weak function of temperature (and \bar{c} is

constant and x_θ is assumed to be so). Consequently, for experiments carried out over a range of temperatures in a regime where this equation holds (*i.e.*, no soft impingement), a plot of $\ln(t_c)$ vs. $(1/T)$ should give a positive slope of a value corresponding to the activation energy for diffusion divided by the universal gas constant.

- (iv) It has been noted earlier that the amount of bainite in a power plant material can vary considerably, even within a given batch of material. Moreover, it is well established that in general x_θ will increase, and the interparticle separation will decrease as the carbon concentration increases. Thus the difference in cementite distribution and structure in a mostly-bainitic microstructure will be very different to that of a mostly-allotriomorphic ferrite microstructure from the same material. The ferrite forms first, enriching with carbon the retained austenite whence the bainite subsequently forms. As a result the effective carbon concentration in the bainite can vary by an order of magnitude, with a dramatic effect on the microstructure of the bainitic region and hence on its ageing behaviour.

Note that the analysis used to produce equation (2.9) is applicable to a plate-like slab of cementite. Bhadeshia (1989) produces a similar analytical approach for spherical cementite, whence, for a particle of radius a , the solute distribution at a given distance ahead of the particle, s , is given by

$$c^\alpha(s, t_c) = \frac{a(\bar{c} - c^{\alpha\theta})}{(a + s)} \operatorname{erfc}\{s/2(D_\alpha t_c)^{0.5}\} \quad (2.10)$$

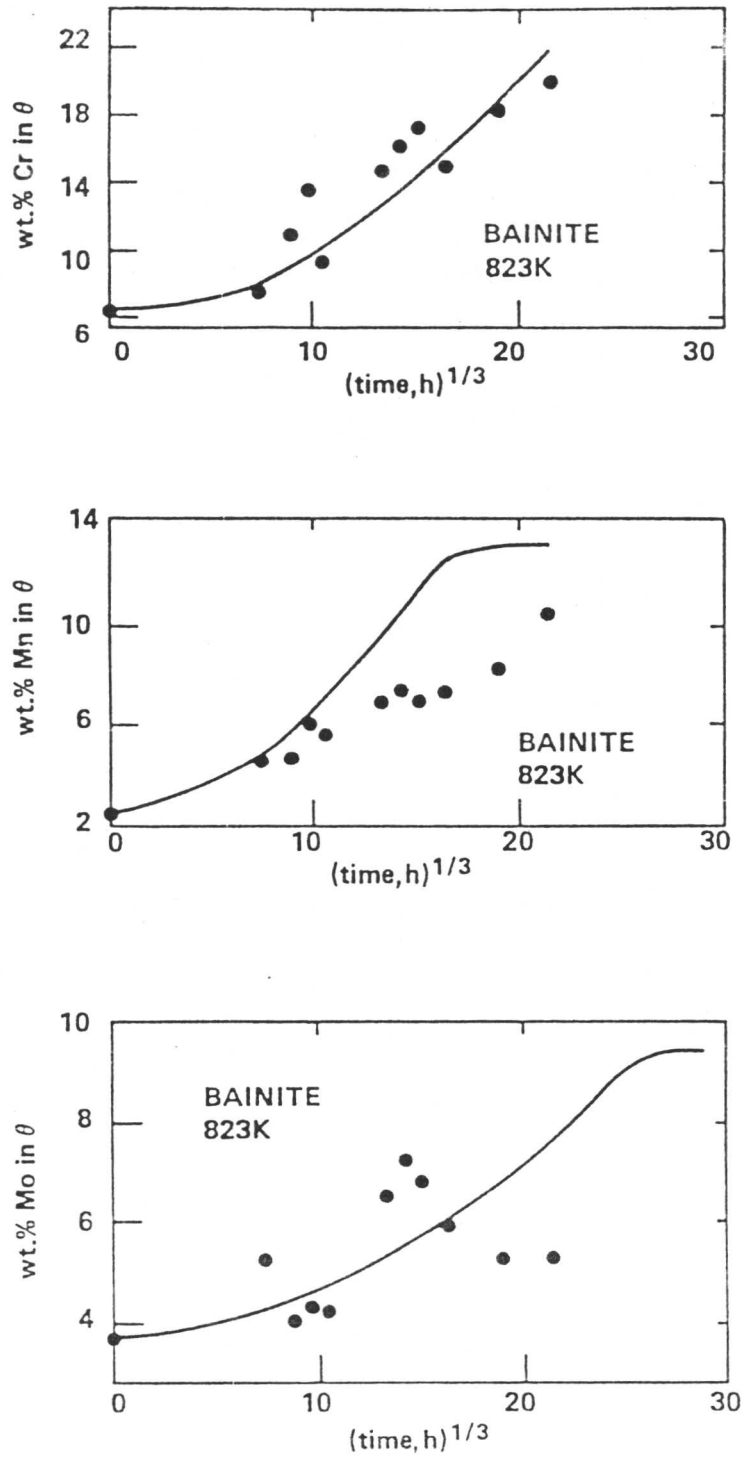


Figure 2.9: A comparison between calculated curves (Bhadeshia, 1989) and experimental data (Afrouz *et al.*, 1983) for the ageing of bainitic cementite in a $1\text{Cr}-\frac{1}{2}\text{Mo}$ type power plant steel

Chapter 3

CHARACTERIZATION OF PRE-SERVICE MICROSTRUCTURE

3.1 Introduction

The objective of this work was to gain a reasonably accurate knowledge of the microstructure of a typical steam header before it had been subjected to service conditions; such a characterization should show the way to a reproduction of such a microstructure by reaustenitizing and transforming back to a mixture of allotriomorphic ferrite and lower bainite. Thence the transformations associated with the production of steam header microstructures could be monitored closely, so as to provide a basis to study the influence of initial transformation conditions and variations in steel composition on the microstructure produced (and hence on the creep properties of the finished artefact). In order to do this it was necessary to characterize the microstructure of the unexposed steam header section as supplied in the as-received condition, and in particular to determine the proportions of the two phases present. Details of the composition of the as-received material, and of the heat treatments used in production of the finished header, can be found in the appendices.

3.2 Optical Metallography

3.2.1 Procedure

Specimens representing both transverse and longitudinal sections of material from the unexposed steam header were prepared. The specimens were mounted in acrylic under hot compression; ground down to 1200 grade emery paper in the first instance; given a final polishing with diamond paste to a minimum of $0.25\mu\text{m}$; and then etched in 2% nital, to bring out the microstructural features. Photography was carried out on an Olympus reflected light microscope using, in most cases, Ilford FP4 (100 ASA) film in the camera and Ilford multigrade paper to produce the positive image (for some of the work at highest magnification a

slower film and high-contrast photographic paper were used in order to improve resolution).

3.2.2 Observed microstructure

Typical micrographs from the transverse section are shown in figures 3.1–3.2, for samples taken from the bore and outer regions of the pipe respectively. Two main microstructural features are apparent: a region of allotriomorphic ferrite, and a region of tempered bainite, containing carbides and ferrite. This is what would have been expected given the heat treatments (appendix).

The ferritic region of these micrographs shows virtually no microscopic detail. This is in accordance with the fact that the intragranular alloy carbide precipitation that accompanies its growth, and which is of such importance to the creep strength and service behaviour of 1Cr– $\frac{1}{2}$ Mo type low-alloy ferritic steel components, is on a very small scale which cannot be resolved optically. The stress relief treatment has not introduced a large degree of coarsening. Some detail in the ferrite was observed occasionally, but it seems quite probable that it was an etching artefact; Rostoker and Dvorak (1977), for example, suggest similar results to the above are attributable to preferential etching in overetched specimens showing segregation of alloying elements to concentrations of dislocations.

One relatively long range feature becomes immediately apparent from an examination of the transverse section micrographs: in the regions nearest to the bore (*i.e.*, the inside surface) of the pipe the microstructure is very strongly banded, that is, the bainitic regions are aligned in rows around the pipe following the circumference. This banding effect is gradually reduced towards the outside of the pipe, becoming indistinguishable at around 15 mm from the bore (distance measured radially), by which point the microstructure ceases to show any degree of alignment with direction. An illustration of the gradual reduction in banding which takes place as the outside of the steam header section is approached is given by figure 3.3.

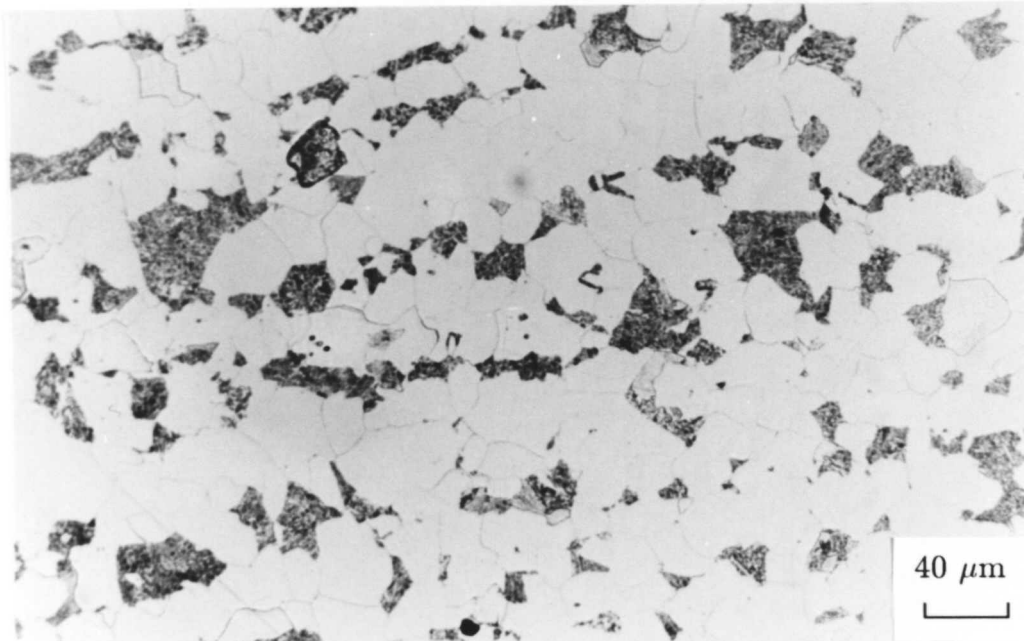
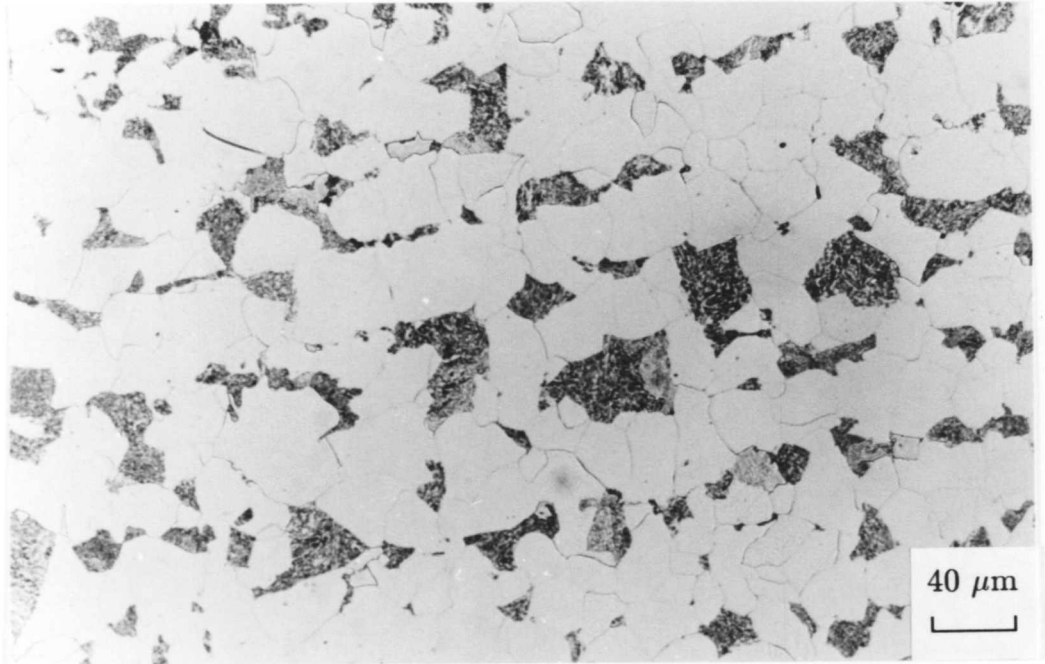


Figure 3.1: Photomicrograph of unexposed steam header material from near to header bore

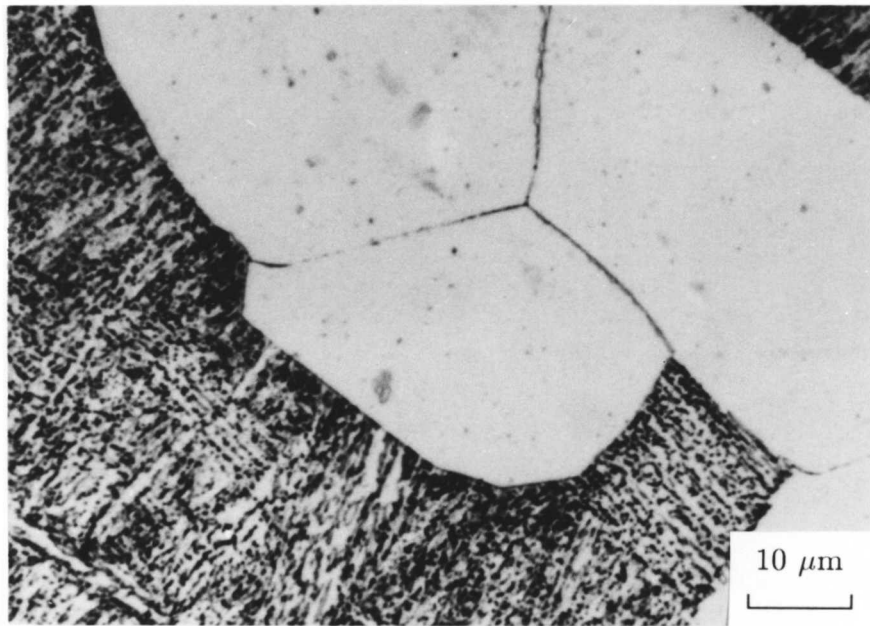
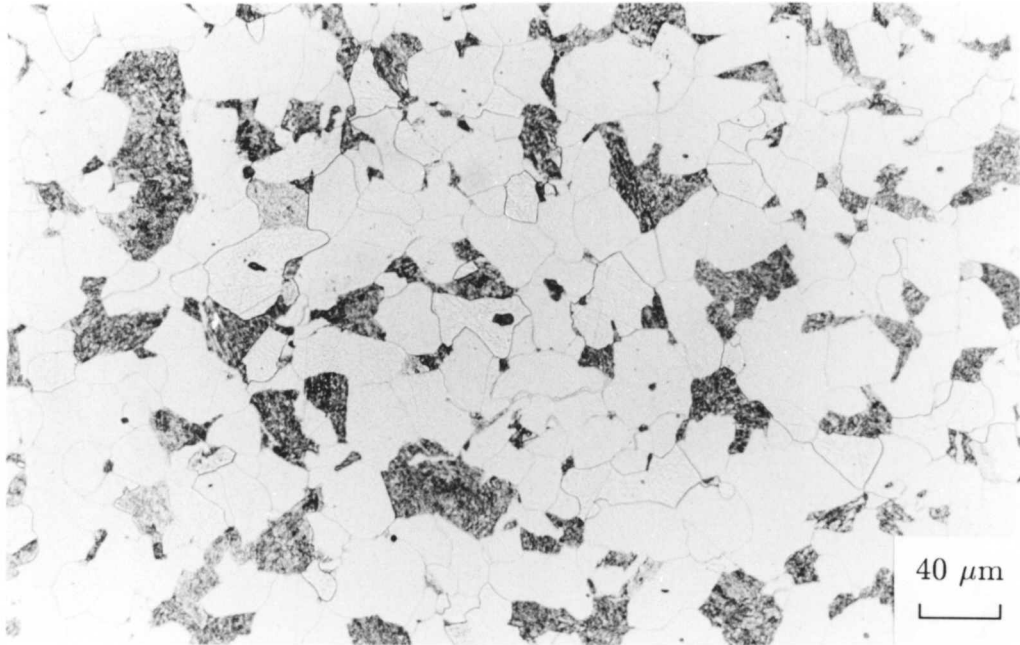
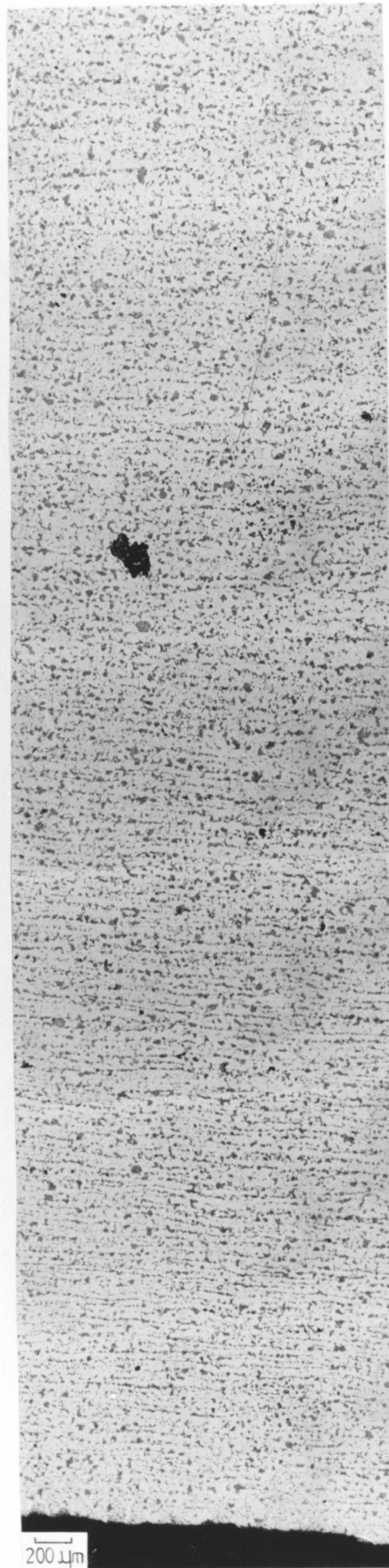


Figure 3.2: Photomicrograph of unexposed steam header material from near to outside surface

Figure 3.3:
Variations in the
microstructure
of the header in
relation to thick-
ness (transverse
section)

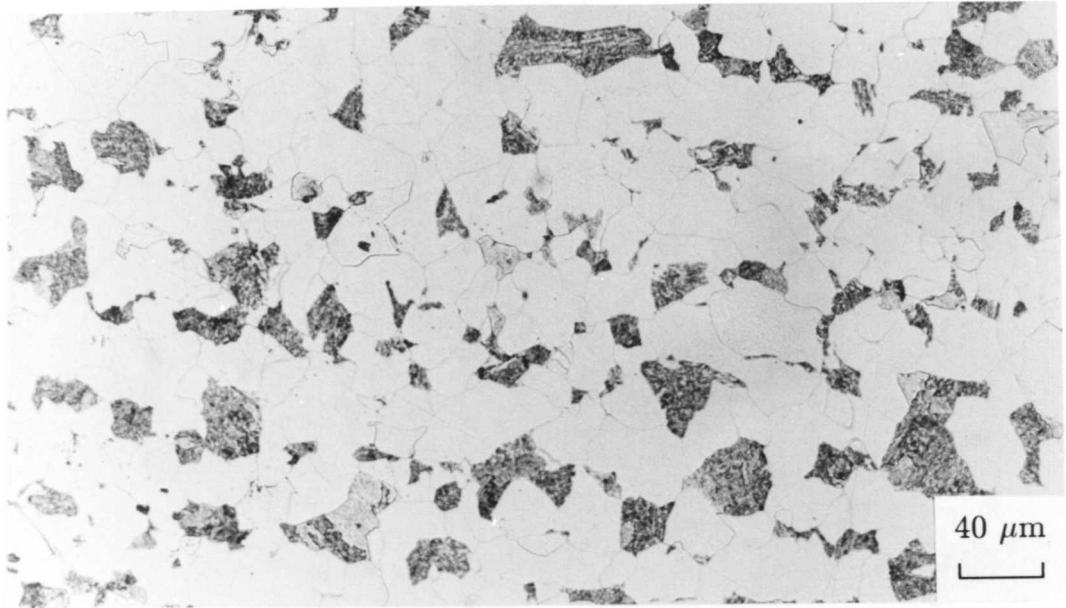


An optical examination of the microstructure alone provides insufficient data to determine with any degree of certainty the cause of the banding effect. Nevertheless, the figure illustrates that the microstructure of steam header material cannot be assumed to be homogeneous. Heterogeneity of microstructure has already been described as a significant cause of error in contemporary remanent life predictive techniques, and it is apparent that a life prediction model for this material which assumed homogeneity of physical properties would produce dubious results, given the observed large scale microstructural differences. Although physical properties, and not mere appearance, govern creep behaviour, the discontinuity of the latter casts doubt on the validity of the conventional assumption of uniformity in the former. The difficulty in quantifying any such heterogeneity, let alone relating it mechanistically to creep behaviour, makes accurate creep life prediction in artefacts with irregular microstructures more difficult.

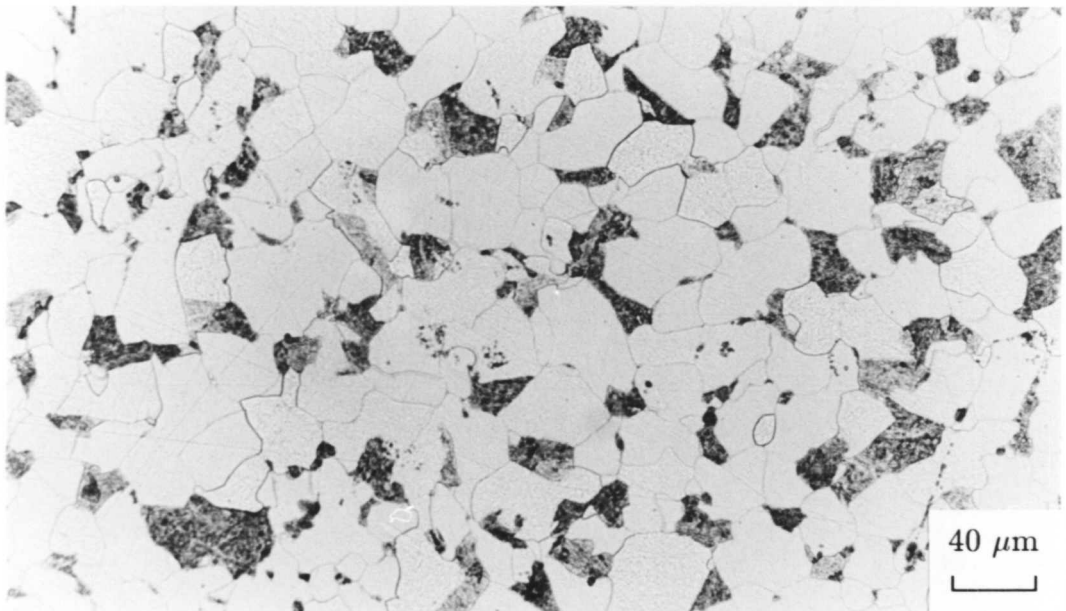
Observations of the specimens prepared from longitudinal sections of the steam header material (*i.e.*, sections cut parallel to the long axis of the pipe) were found to be similar to the observations made from the transverse sections (*i.e.*, mixed ferrite/bainite with some microstructural detail within the ferrite grains which may be suggestive of intragranular carbide precipitation) (figure 3.4).

3.3 Quantitative Metallography

A quantitative representation of the relative proportions of ferrite and bainite was obtained using a point counter. It was necessary to record 700–800 points for each area of the material before results of satisfactory statistical significance could be obtained. In order to obtain a representative sample with the microstructure partially aligned as it is in the bore region of the as-received steam header material, the data were obtained from a number of random specimen orientations. An optical specimen was given the lightest possible etching which still allowed the phases to be distinguished, as the point counting tech-



Near bore



Away from bore

Figure 3.4: Photomicrographs of unexposed steam header in longitudinal section

nique requires that measurements are made on a two dimensional section, and excessive etching so that one phase is significantly in relief would cause this condition to break down.

The microstructure was found to be 25% bainitic in the region near the bore, but with an increased percentage of bainite, 28%, near the edge. Gladman & Woodhead (1960) have shown that the standard deviation, σ_V , of the volume fraction measured by a point counting method, V_v , is given by the following relationship:

$$\left(\frac{\sigma_V}{V_v}\right)^2 = \frac{1 - V_v}{N} \quad (3.1)$$

where N is the total number of readings taken. It follows that the standard error at the 95% level, $2\sigma_V$, is determined by equation (3.2):

$$2\sigma_V = 2V_v \sqrt{\frac{1 - V_v}{N}} \quad (3.2)$$

This produces 95% confidence limits in the measured values for volume fraction of 1.4% for the bore region value and 1.6% for the outer region value; therefore, the measured difference in volume fraction is a statistically-significant feature, and a further indication of long-range microstructural inhomogeneity in the as-received steam header material.

3.4 Hardness Measurements

3.4.1 Microhardness testing

Microhardness measurements were made at different points in the material for both longitudinal and transverse section specimens. Readings for the ferritic and bainitic regions of the as-received microstructure were considered separately.

Testing was carried out on polished specimens given as light an etch as possible (so that the bainite could be distinguished, but without introducing too much surface roughness and other surface artefacts). A Leitz indenter equipped